Journal of Computational Physics 544 (2026) 114402

Contents lists available at ScienceDirect

Journal of Computational Physics

journal homepage: www.elsevier.com/locate/jcp

Exponential supplementary variable methods for complex-valued Hamiltonian PDEs with applications to rotating Gross–Pitaevskii equation

Yuezheng Gong [a], Chaolong Jiang [b,*], Yong Zhang [c]

[a] School of Mathematics, Nanjing University of Aeronautics and Astronautics, Nanjing, 211106, China
[b] School of Statistics and Mathematics, Yunnan University of Finance and Economics, Kunming, 650221, China
[c] Center for Applied Mathematics and KL-AAGDM, Tianjin University, Tianjin, 300072, China

ARTICLE INFO

Keywords:
Exponential supplementary variable methods
Complex-valued Hamiltonian partial differential equations
Lawson Runge–Kutta methods
Prediction-correction techniques

ABSTRACT

In this paper, we propose an exponential supplementary variable method, ingeniously merging the supplementary variable method initially conceived for gradient flows Gong et al.(2021), Hong et al. (2023) with the Lawson transform methodology Hochbruck and Ostermann (2010), to preserve multiple conserved quantities for complex-valued Hamiltonian partial differential equations. We first reformulate the original system by introducing several supplementary *scalar* variables, which are equal to zero on the analytical level, to enforce the multiple conservation laws. Then, leveraging the Lawson transform framework, we develop a novel class of highly efficient high-order exponential integrators utilizing prediction and correction Lawson Runge–Kutta schemes. The multiple conservation laws are preserved on the discrete level by solving a set of scalar algebraic equations, which can be efficiently computed via iterative methods. The proposed methods manifest a better numerical performance in terms of accuracy, efficiency and long-term simulation. To substantiate their precision, effectiveness, and overarching excellence, we apply these methods to the Gross–Pitaevskii equation, multi-component Gross–Pitaevskii equations and Schrödinger–Poisson equation, showcasing their prowess in simulating intricate dynamics such as the evolution of a quantized vortex lattice within a rotating Bose–Einstein condensate.

1. Introduction

Complex-valued Hamiltonian partial differential equations (PDEs) have a wide range of applications in the fields of science and engineering. They provide the mathematical framework for a diversity of physical phenomena, extending from fluid mechanics and quantum mechanics to nonlinear optics [4]. The general form can be articulated in the following manner

$$\partial_t z = \mathcal{S}(z)\frac{\delta \mathcal{E}}{\delta z^*}, \tag{1.1}$$

where $z = z(\mathbf{x}, t)$ is a complex-valued function, $(\mathbf{x}, t) \in D \times (0, T] \subset \mathbb{R}^d \times \mathbb{R}$, $\mathcal{S}(z)$ is a structured skew-Hermitian operator, variable z^* is the complex conjugate of z and $\frac{\delta \mathcal{E}}{\delta z^*}$ denotes the variational derivative of the Hamiltonian energy $\mathcal{E}$ with respect to z^*. Within Hamiltonian systems, it is typical to have at least one, and frequently multiple, conserved quantities that align with the preservation of energy, momentum, and other analogous physical principles. Consequently, there is a strong imperative to devise numerical methods capable of maintaining these conserved quantities.

* Corresponding author.
E-mail addresses: gongyuezheng@nuaa.edu.cn (Y. Gong), zz2048@ynufe.edu.cn (C. Jiang), Zhang_Yong@tju.edu.cn (Y. Zhang).

https://doi.org/10.1016/j.jcp.2025.114402
Received 24 February 2025; Received in revised form 3 August 2025; Accepted 23 September 2025
Available online 10 October 2025

Numerical schemes that conserve invariants or first integrals have been shown to be extremely beneficial for studying the long-time behavior of dynamical systems. Such schemes are commonly called energy-preserving or integral-preserving methods [5,6]. Over the past few decades, numerous energy-preserving methods have been developed for Hamiltonian ordinary differential equations (ODEs), including discrete gradient (DG) methods [7], averaged vector field (AVF) methods [8], energy-preserving variant of collocation methods [9] and Hamiltonian boundary value methods [10], etc. It is natural to generalize the energy-preserving algorithms from Hamiltonian ODEs to Hamiltonian PDEs through appropriate spatial discretization. Furihata [11] extended DG methods to Hamiltonian PDEs and introduced discrete variational derivative methods. Celledoni et al. [12] utilized the AVF method to give a systematic energy-preserving scheme for Hamiltonian PDEs. Additionally, specific projection techniques were proposed to devise structure-preserving schemes that maintain multiple invariants [13,14]. However, the dominant linear operator of the complex-valued Hamiltonian PDEs is usually skew-Hermitian with eigenvalues of very large modulus. Traditional energy-preserving methods cannot contain the full information of the linear operator, and they may suffer from a very severe time step limitation and can not guarantee convincing results in the long-time simulations.

In [3], it was pointed out that another type of time integration scheme called exponential integrators could address this problem well. There has been great interest in devising energy-preserving exponential integrators over the past few decades. The most natural way is to first rewrite the original system in an equivalent form using the Lawson transform [15] or variation-of-constants formula, and then apply a classical integrator for the equivalent system [16,17]. For example, Celledoni et al. [18] presented a class of high-order symmetric exponential integrator schemes. Bhatt et al. [19] derived exponential Runge–Kutta (RK) schemes to preserve the decay rates exactly for both linear and quadratic invariants. Recently, by modifying the integrator theory, Mei et al. [20] derived a fourth-order energy-preserving exponential AVF scheme. These existing schemes are usually fully implicit and nonlinear, and there is no existing theory on the convergence of the iterative algorithm for now.

Compared with fully implicit schemes, linearly implicit methods only require to solve a linear system. Thus, the computational cost is significantly reduced. In addition, the theory on the convergence of iterative algorithm for the linear equations are well established. Combining the quadratic polarization approach presented in Dahlby and Owren [5] with the exponential integrator, a multistep linearly implicit energy-preserving exponential scheme is presented for polynomial Hamiltonian PDEs [21]. One disadvantage of such method is that it is not valid for general Hamiltonian PDEs and usually cannot conserves multiple invariants. Based on the idea of energy quadratization (EQ) approaches [22,23] firstly proposed for developing efficient energy stable schemes of gradient flows and the Lawson transformation, Jiang et al. [24] presented a high-order linearly implicit energy-preserving exponential scheme for the nonlinear Schrödinger equation, where the energy conservation law was achieved with respect to a modified quadratic energy. More recently, Li et al. [25] presented a class of energy-conserving exponential Rosenbrock methods for oscillatory Hamiltonian systems, which conserved only a single quantity. However, the search for bona fide efficiently high-order exponential integrator methods that allow for multiple conserved quantities is still ongoing.

In [26,27], Cheng and Shen proposed a new Lagrange multiplier (LM) approach for gradient flows where they successfully achieved unconditional energy stability. Later, Gong et al. [1,2] promoted it further and introduced supplementary variable method (SVM), wherein the gradient flow problem was reformulated into a constraint-free system by introducing some supplementary variables whose number is the same as the inherent dissipation laws and constraints. The dissipation laws are given explicitly thanks to the supplementary variables, therefore, it is more convenient and flexible to develop high-order schemes for gradient flows.

Despite such great success in gradient flows, there are quite few literature focusing on Hamiltonian systems, for example, the Bose–Einstein condensation (BEC) [28]. So far as we known, Antoine, Shen and Tang combined SAV and LM for the nonlinear Schrödinger equation [29], wherein the numerical mass and energy preservation are guaranteed for a very small time step, thus the long-time simulation is quite challenging in terms of efficiency. In fact, on the one hand, it seems quite natural to adapt SVM for BEC problems since conserved quantities, e.g., mass and energy, can be viewed as equality-type constraints. On the other hand, similar to traditional energy-preserving methods, a direct naive extension of SVM *does not* make full use of the dominant linear operator, which is essentially the main source rendering highly oscillatory property and shall enforce a prohibitively small CFL condition number. To alleviate the stringent time step restriction, as pointed out in Hochbruck and Ostermann [3], Besse et al. [30], an inclusion of the dominant linear operator via the 'exponential integrator' is of great importance, and will help improve not only numerical stability but also the accuracy, efficiency and long-time simulation performance.

In this paper, we choose to combine SVM and the Lawson transformation method, a typical exponential integrator, so to develop an exponential supplementary variable method (ESVM). The proposed method allows for preservation of multiple conserved quantities, similar to SVM, and manifests a better numerical performance due to the adoption of exponential integrator. We analyze the local existence and uniqueness together with convergence order rigorously, and study three typical complex-valued Hamiltonian PDEs (1.1), i.e., Gross–Pitaevskii (GP) equation, multi-component GP equations and Schrödinger–Poisson (SP) equation. A comprehensive comparison with existing structure-preserving methods in terms of the accuracy, efficiency as well as long-time simulation and applications to simulate a quantized vortex lattice dynamics in a rotating BEC are reported.

Overall, the key novelties of our method are summarized as follows:

1. It produces a new class of high-order exponential integrators, which can preserve multiple invariants, and can be easily extended to general Hamiltonian PDEs.
2. It involves solving a very small algebraic equation system with variable number equal to the number of conserved quantities, and such system can be computed by iterative solver efficiently.
3. It allows for a relatively large time step due to the exact integration of the linear part.

The rest of this paper is structured as follows. In Section 2, the ESVM reformulation for complex-valued Hamiltonian PDEs is introduced. In Sections 3, a novel class of high-order energy-preserving ESVM algorithms is presented and some theoretical results are given. In Section 4, various numerical experiments are shown to demonstrate the accuracy, efficiency and long-time evolution of mass and energy conservation laws. Conclusions are drawn in Section 5.

2. ESVM reformulation

In this section, we introduce the ESVM reformulation for general complex-valued PDEs with multiple conserved quantities. For brevity, we only present the ESVM reformulation for two conserved quantities case, and its extension to multiple conserved quantities case is trivial.

To begin with, we shall first establish the equivalence between ESVM-reformulated system and the original model. Introduce the inner product in $L^2(D)$ as

$$(f, g) = \int_D f(\mathbf{x})\, g^*(\mathbf{x})\mathrm{d}\mathbf{x},$$

where $f(\mathbf{x})$, $g(\mathbf{x}) \in L^2(D)$, $g^*(\mathbf{x})$ is the complex conjugate of function $g(\mathbf{x})$. Correspondingly, the norm in $L^2(D)$ is denoted by $\|f\| = \sqrt{(f, f)}$. We rewrite (1.1) as follows

$$\partial_t z = \mathcal{L} z + \mathcal{N}[z], \tag{2.1}$$

where $z = z(\mathbf{x}, t)$ is a complex-valued function, $\mathcal{L}$ is usually a linear skew-Hermitian operator admitting eigenvalues of large modulus and $\mathcal{N}[z]$ is a nonlinear functional. As stated above, Hamiltonian PDEs admit at least one and often multiple conserved quantities. Let us assume that the system (2.1) adheres to both energy and mass conservation laws

$$\frac{\mathrm{d}}{\mathrm{d}t}\mathcal{E} = 0, \quad \frac{\mathrm{d}}{\mathrm{d}t}\mathcal{M} = 0, \tag{2.2}$$

where $\mathcal{E} = \mathcal{E}[z]$ and $\mathcal{M} = \mathcal{M}[z]$ represent the total energy and mass respectively. Therefore, the vector field of (2.1) satisfies

$$\mathfrak{R}\Big(\mathcal{L} z + \mathcal{N}[z], \frac{\delta \mathcal{E}}{\delta z^*}\Big) = 0, \quad \mathfrak{R}\Big(\mathcal{L} z + \mathcal{N}[z], \frac{\delta \mathcal{M}}{\delta z^*}\Big) = 0.$$

Applying the SVM reformulation for the system (2.1) with the two conservation laws (2.2), we obtain the following reformulated system

$$\begin{cases} \partial_t z = \mathcal{L} z + \mathcal{N}[z] + \alpha_1 g_1[z] + \alpha_2 g_2[z], \\ \dfrac{\mathrm{d}}{\mathrm{d}t}\mathcal{E} = 0, \ \dfrac{\mathrm{d}}{\mathrm{d}t}\mathcal{M} = 0, \end{cases} \tag{2.3}$$

where α_1 and α_2 are two real supplementary variables, and $g_1[z]$ and $g_2[z]$ are two complex-valued user-supplied functionals. Next, using Lawson transformation

$$Z = \exp(-t\mathcal{L})z,$$

we transform (2.3) into the ESVM reformulation

$$\begin{cases} \partial_t Z = \exp(-t\mathcal{L})\mathcal{N}[z] + \alpha_1 \exp(-t\mathcal{L}) g_1[z] + \alpha_2 \exp(-t\mathcal{L}) g_2[z], \\ \dfrac{\mathrm{d}}{\mathrm{d}t}\mathcal{E} = 0, \ \dfrac{\mathrm{d}}{\mathrm{d}t}\mathcal{M} = 0, \ z = \exp(t\mathcal{L})Z. \end{cases} \tag{2.4}$$

As noted, the Lawson transformation is reversible simply because $\mathcal{L}$ is a linear skew-Hermitian operator. It is important to note that the above ESVM reformulation lays a solid mathematical foundation for developing robust, highly efficient and accurate exponential structure-preserving algorithms. To check the consistence of (2.4) and (2.1), we introduce the following consistency matrix

$$\boldsymbol{J}[z] = \begin{pmatrix} \mathfrak{R}\Big(g_1[z], \frac{\delta \mathcal{E}}{\delta z^*}\Big) & \mathfrak{R}\Big(g_2[z], \frac{\delta \mathcal{E}}{\delta z^*}\Big) \\ \mathfrak{R}\Big(g_1[z], \frac{\delta \mathcal{M}}{\delta z^*}\Big) & \mathfrak{R}\Big(g_2[z], \frac{\delta \mathcal{M}}{\delta z^*}\Big) \end{pmatrix}. \tag{2.5}$$

Theorem 1. *If the consistency matrix $\boldsymbol{J}[z]$ is nonsingular, the ESVM reformulation (2.4) is equivalent to the original system (2.1).*

Proof. By virtue of

$$\Big(\frac{\delta \mathcal{E}}{\delta z}\Big)^* = \frac{\delta \mathcal{E}}{\delta z^*}, \quad \mathfrak{R}\Big(\mathcal{L} z + \mathcal{N}[z], \frac{\delta \mathcal{E}}{\delta z^*}\Big) = 0,$$

we induce from the system (2.3) that

$$\begin{aligned} 0 = \frac{\mathrm{d}}{\mathrm{d}t}\mathcal{E} &= \int_D \Big(\frac{\delta \mathcal{E}}{\delta z} \cdot z_t + \frac{\delta \mathcal{E}}{\delta z^*} \cdot z_t^*\Big)\mathrm{d}\mathbf{x} \\ &= \Big(z_t, \frac{\delta \mathcal{E}}{\delta z^*}\Big) + \Big(\frac{\delta \mathcal{E}}{\delta z^*}, z_t\Big) = 2\mathfrak{R}\Big(z_t, \frac{\delta \mathcal{E}}{\delta z^*}\Big) \end{aligned}$$

$$= 2\Re\Big(\mathcal{L}z + \mathcal{N}[z] + \alpha_1 g_1[z] + \alpha_2 g_2[z], \frac{\delta\mathcal{E}}{\delta z^*}\Big)$$
$$= 2\alpha_1\Re\Big(g_1[z], \frac{\delta\mathcal{E}}{\delta z^*}\Big) + 2\alpha_2\Re\Big(g_2[z], \frac{\delta\mathcal{E}}{\delta z^*}\Big).$$

By the same token, we have

$$0 = \frac{\mathrm{d}}{\mathrm{d}t}\mathcal{M} = 2\alpha_1\Re\Big(g_1[z], \frac{\delta\mathcal{M}}{\delta z^*}\Big) + 2\alpha_2\Re\Big(g_2[z], \frac{\delta\mathcal{M}}{\delta z^*}\Big).$$

From the above two equations, we have $J[z]\boldsymbol{\alpha} = \mathbf{0}$. It immediately implies $\alpha_1 = \alpha_2 = 0$ if the consistency matrix $J[z]$ is nonsingular. So, we conclude that SVM reformulation (2.3) is equivalent to the original system (2.1). Since (2.4) is a equivalent formulation of the SVM Eq. (2.3), we then complete the proof. □

Corollary 1. *If we take* $g_1[z] = \frac{\delta\mathcal{E}}{\delta z^*}$ *and* $g_2[z] = \frac{\delta\mathcal{M}}{\delta z^*}$*, and further assume that* $\frac{\delta\mathcal{E}}{\delta z^*}$ *and* $\frac{\delta\mathcal{M}}{\delta z^*}$ *are linearly independent, then the ESVM reformulation* (2.4) *is equivalent to the original system* (2.1)*.*

Proof. As $g_1[z] = \frac{\delta\mathcal{E}}{\delta z^*}$ and $g_2[z] = \frac{\delta\mathcal{M}}{\delta z^*}$, we have

$$J[z] = \begin{pmatrix} \|\frac{\delta\mathcal{E}}{\delta z^*}\|^2 & \Re\Big(\frac{\delta\mathcal{M}}{\delta z^*}, \frac{\delta\mathcal{E}}{\delta z^*}\Big) \\ \Re\Big(\frac{\delta\mathcal{E}}{\delta z^*}, \frac{\delta\mathcal{M}}{\delta z^*}\Big) & \|\frac{\delta\mathcal{M}}{\delta z^*}\|^2 \end{pmatrix}.$$

The above matrix is nonsingular if and only if $\frac{\delta\mathcal{E}}{\delta z^*}$ and $\frac{\delta\mathcal{M}}{\delta z^*}$ are linearly independent. □

One typical example of (2.1) is the well-known nonlinear GP equation

$$\begin{cases} \mathrm{i}\frac{\partial}{\partial t}\psi = \Big[-\frac{1}{2}\Delta + V(\mathbf{x}) - \Omega L_z + \beta|\psi|^2\Big]\psi, \quad t > 0, \\ \psi(\mathbf{x}, 0) = \psi_0(\mathbf{x}), \qquad \mathbf{x} \in \mathbb{R}^2, \end{cases} \tag{2.6}$$

where t is the time variable, $\mathbf{x}$ is the spatial variable, $\mathrm{i} = \sqrt{-1}$ is the complex unit, $\psi = \psi(\mathbf{x}, t)$ is the complex-valued wave function, Δ is the Laplace operator, $\Omega L_z = -\mathrm{i}\Omega(x\partial_y - y\partial_x)$ represents the angular momentum rotational term, β represents the local interaction strength, and $\psi_0(\mathbf{x})$ is the initial profile. The external potential is taken as the harmonic potential

$$V(\mathbf{x}) = \frac{1}{2}\Big(\gamma_x^2 x^2 + \gamma_y^2 y^2\Big), \tag{2.7}$$

with $\gamma_x > 0, \gamma_y > 0$ being the trapping frequencies in the x and y direction respectively.

The GP Eq. (2.6) can be rewritten as

$$\partial_t\psi = \mathcal{L}\psi + \mathcal{N}[\psi], \tag{2.8}$$

where $\mathcal{L} = \frac{\mathrm{i}}{2}\Delta$ and $\mathcal{N}[\psi] = -\mathrm{i}\big[V(\mathbf{x}) - \Omega L_z + \beta|\psi|^2\big]\psi$. It conserves the energy

$$\mathcal{E}[\psi] = \int_{\mathbb{R}^2}\Big(-\frac{1}{2}|\nabla\psi|^2 - V|\psi|^2 - \frac{\beta}{2}|\psi|^4 + \Omega\psi^* L_z\psi\Big)\mathrm{d}\mathbf{x}, \tag{2.9}$$

and total mass $\mathcal{M}[\psi] = \int_{\mathbb{R}^2}|\psi(\mathbf{x}, t)|^2\mathrm{d}\mathbf{x}$. The ESVM reformulation of (2.6) reads as

$$\begin{cases} \partial_t\Psi = \exp(-\frac{\mathrm{i}t}{2}\Delta)\mathcal{N}[\psi] + \alpha_1\exp(-\frac{\mathrm{i}t}{2}\Delta)g_1[\psi] + \alpha_2\exp(-\frac{\mathrm{i}t}{2}\Delta)g_2[\psi], \\ \frac{\mathrm{d}}{\mathrm{d}t}\mathcal{E} = 0, \quad \frac{\mathrm{d}}{\mathrm{d}t}\mathcal{M} = 0, \quad \psi(\mathbf{x}, t) = \exp(\frac{\mathrm{i}t}{2}\Delta)\Psi(\mathbf{x}, t), \end{cases} \tag{2.10}$$

where

$$g_1[\psi] = \frac{\delta\mathcal{E}}{\delta\psi^*} = \Big(\frac{1}{2}\Delta - V(\mathbf{x}) + \Omega L_z - \beta|\psi|^2\Big)\psi, \qquad g_2[\psi] = \frac{\delta\mathcal{M}}{\delta\psi^*} = \psi.$$

Another typical example of (2.1) is Schrödinger–Poisson (SP) equation [31]

$$\begin{cases} \mathrm{i}\frac{\partial}{\partial t}\psi = \Big[-\frac{1}{2}\Delta + V(\mathbf{x}) - \Omega L_z + \alpha\Phi(\mathbf{x}, t) + \beta|\psi|^2\Big]\psi, \\ \Delta\Phi(\mathbf{x}, t) = -|\psi(\mathbf{x}, t)|^2, \quad t > 0, \\ \psi(\mathbf{x}, 0) = \psi_0(\mathbf{x}), \qquad \mathbf{x} \in \mathbb{R}^2, \end{cases} \tag{2.11}$$

which can be reformulated as

$$\mathrm{i}\frac{\partial}{\partial t}\psi = \Big[-\frac{1}{2}\Delta + V(\mathbf{x}) - \Omega L_z + \alpha\Phi(|\psi|^2) + \beta|\psi|^2\Big]\psi. \tag{2.12}$$

The Poisson potential Φ is given explicitly by the convolution of density $|\psi|^2$ and kernel $U(\mathbf{x}) = -\frac{1}{2\pi}\ln(|\mathbf{x}|)$, as follows

$$\Phi(|\psi|^2) = U(\mathbf{x}) * |\psi(\mathbf{x}, t)|^2 = [U * \rho](\mathbf{x}). \tag{2.13}$$

Table 1
The coefficients of Lawson RK method (3.1).

$$\begin{array}{c|c|c} c & \mathrm{A} & \varphi \\ \hline & b^{\top} & \varphi_0 \end{array} = \begin{array}{c|ccc|c} c_1 & a_{11} & \cdots & a_{1s}\exp\big((c_1-c_s)\tau\mathcal{L}\big) & \exp(c_1\tau\mathcal{L}) \\ \vdots & \vdots & \ddots & \vdots & \vdots \\ c_s & a_{s1}\exp\big((c_s-c_1)\tau\mathcal{L}\big) & \cdots & a_{ss} & \exp(c_s\tau\mathcal{L}) \\ \hline & b_1\exp\big((1-c_1)\tau\mathcal{L}\big) & \cdots & b_s\exp\big((1-c_s)\tau\mathcal{L}\big) & \exp(\tau\mathcal{L}) \end{array}$$

The SP Eq. (2.12) can be rewritten as

$$\partial_t\psi = \mathcal{L}\psi + \mathcal{N}[\psi], \tag{2.14}$$

where $\mathcal{L} = \frac{\mathrm{i}}{2}\Delta$ and $\mathcal{N}[\psi] = -\mathrm{i}\big[V(\mathbf{x}) - \Omega L_z + \alpha\Phi(|\psi|^2) + \beta|\psi|^2\big]\psi$. Similarly, Eq. (2.12) conserves both energy

$$\mathcal{E}[\psi] = \int_{\mathbb{R}^2}\left(-\frac{1}{2}|\nabla\psi|^2 - V(\mathbf{x})|\psi|^2 - \frac{\alpha}{2}\Phi|\psi|^2 - \frac{\beta}{2}|\psi|^4 + \Omega\psi^* L_z\psi\right)\mathrm{d}\mathbf{x}, \tag{2.15}$$

and the total mass $\mathcal{M}[\psi] = \int_{\mathbb{R}^2}|\psi(x,t)|^2\mathrm{d}x$. The ESVM reformulation is given by

$$\begin{cases} \partial_t\Psi = \exp(-\frac{\mathrm{i}t}{2}\Delta)\mathcal{N}[\psi] + \alpha_1\exp(-\frac{\mathrm{i}t}{2}\Delta)g_1[\psi] + \alpha_2\exp(-\frac{\mathrm{i}t}{2}\Delta)g_2[\psi], \\ \frac{\mathrm{d}}{\mathrm{d}t}\mathcal{E} = 0, \quad \frac{\mathrm{d}}{\mathrm{d}t}\mathcal{M} = 0, \quad \psi(x,t) = \exp(\frac{\mathrm{i}t}{2}\Delta)\Psi(x,t), \end{cases} \tag{2.16}$$

with

$$g_1[\psi] = \frac{\delta\mathcal{E}}{\delta\psi^*} = \Big(\frac{1}{2}\Delta - V(\mathbf{x}) + \Omega L_z - \alpha\Phi - \beta|\psi|^2\Big)\psi, \qquad g_2[\psi] = \frac{\delta\mathcal{M}}{\delta\psi^*} = \psi.$$

Remark 1. As stated in Ref. [30], the choice of $\mathcal{L}$ is somewhat flexible as long as its exponential operator ($e^{t\mathcal{L}}$) can be computed efficiently. In this article, we choose $\mathcal{L} = \frac{\mathrm{i}}{2}\Delta$ and efficiently compute $e^{t\mathcal{L}}\psi$ in Fourier space. One may also consider $\mathcal{L} = \frac{\mathrm{i}}{2}\Delta - \mathrm{i}V(\mathbf{x}) + \mathrm{i}\Omega L_z$, and its exponential operator can be computed with great efficiency following a similar exact-splitting Fourier spectral method as shown in Liu et al. [32]. We shall report the results later in a future work.

3. High-order mass and energy-preserving scheme

In this section, based on the ESVM reformulation (2.4), we will show how to systematically develop highly efficient and high-order exponential structure-preserving schemes. To start with, we shall recall some common knowledge on prediction-correction Runge–Kutta scheme.

3.1. Prediction-correction Lawson scheme

In this subsection, we shall collect some common and useful results on a class of semi-discrete Lawson Runge–Kutta (RK) schemes for system (2.1).

Definition 1 (Lawson RK Method)**.** Let b_i, a_{ij} $(i,j = 1,\dots,s)$ be real numbers and $c_i = \sum_{j=1}^{s} a_{ij}$. An s-stage Lawson RK method is given by

$$\begin{cases} z_{ni} = \exp(c_i\tau\mathcal{L})z^n + \tau\sum_{j=1}^{s} a_{ij}\exp\big((c_i-c_j)\tau\mathcal{L}\big)\mathcal{N}[z_{nj}], \\ z^{n+1} = \exp(\tau\mathcal{L})z^n + \tau\sum_{i=1}^{s} b_i\exp((1-c_i)\tau\mathcal{L})\mathcal{N}[z_{ni}]. \end{cases} \tag{3.1}$$

In general, the coefficients are displayed as follows [3] (Table 1):

The above Lawson Runge–Kutta method (3.1) shall be reduced to a classical RK method if $\mathcal{L} = 0$, and the classical method will be henceforth referred to as the underlying Runge–Kutta method [3]. If the underlying RK method is implicit, the corresponding Lawson RK method (2) is implicit too. In numerical practice, solving an implicit scheme poses significant challenges since it often requires to design an iterative solver for the large-scale nonlinear equations, leading to considerable computational costs or even unexpected divergence. To mitigate such problem, one approach is to utilize the prediction-correction technique, which also facilitates the development of prediction-correction Lawson RK method.

Theorem 2 (Convergence order [15])**.** *If the underlying RK method is of order p, then the Lawson RK method (3.1) is also of order p.*

Scheme 3.1 (Prediction-Correction Lawson RK method)**.** Let b_i, a_{ij} $(i,j = 1,\dots,s)$ be real numbers and $c_i = \sum_{j=1}^{s} a_{ij}$. An s-stage prediction-correction Lawson RK method is defined as

- **Prediction:** let $z_{ni}^{(0)} = \exp(c_i\tau\mathcal{L})z^n$ and M be a given positive integer, we explicitly calculate $z_{ni}^{(\ell+1)}$ from $\ell = 0$ to $M-1$ as follows

$$z_{ni}^{(\ell+1)} = \exp(c_i\tau\mathcal{L})z^n + \tau\sum_{j=1}^{s} a_{ij}\exp\big((c_i-c_j)\tau\mathcal{L}\big)\mathcal{N}[z_{nj}^{(\ell)}]. \tag{3.2}$$

- **Correction:** we update $z^{n+1,(M)}$ as

$$z^{n+1,(M)} = \exp(\tau\mathcal{L})z^n + \tau\sum_{i=1}^{s} b_i\exp((1-c_i)\tau\mathcal{L})\ \mathcal{N}[z_{ni}^{(M)}]. \tag{3.3}$$

By a similar argument as the proof of Theorem 3.1 in Ref. [2], we obtain the following theorem.

Theorem 3. *Assume that z^{n+1} and $z^{n+1,(M)}$ are solutions to Eq. (3.1) and Scheme 3.1 respectively, we have*

$$z^{n+1} = z^{n+1,(M)} + \mathcal{O}(\tau^{M+2}).$$

Remark 2. For sake of clarity, we list some typical and also very important examples, including the second and fourth order schemes, for later discussion.

- A second-order prediction-correction Lawson RK method ($M \geq 1$) is

$$\begin{array}{c|c|c} \frac{1}{2} & \frac{1}{2} & \exp(\frac{\tau}{2}\mathcal{L}) \\ \hline & \exp(\frac{\tau}{2}\mathcal{L}) & \exp(\tau\mathcal{L}) \end{array}.$$

.

- A fourth-order prediction-correction Lawson RK method ($M \geq 3$) reads as

$$\begin{array}{c|cc|c} \frac{1}{2}-\frac{\sqrt{3}}{6} & \frac{1}{4} & (\frac{1}{4}-\frac{\sqrt{3}}{6})\exp(-\frac{\sqrt{3}}{3}\tau\mathcal{L}) & \exp\big((\frac{1}{2}-\frac{\sqrt{3}}{6})\tau\mathcal{L}\big) \\ \frac{1}{2}+\frac{\sqrt{3}}{6} & (\frac{1}{4}+\frac{\sqrt{3}}{6})\exp(\frac{\sqrt{3}}{3}\tau\mathcal{L}) & \frac{1}{4} & \exp\big((\frac{1}{2}+\frac{\sqrt{3}}{6})\tau\mathcal{L}\big) \\ \hline & \frac{1}{2}\exp\big((\frac{1}{2}+\frac{\sqrt{3}}{6})\tau\mathcal{L}\big) & \frac{1}{2}\exp\big((\frac{1}{2}-\frac{\sqrt{3}}{6})\tau\mathcal{L}\big) & \exp(\tau\mathcal{L}) \end{array}.$$

3.2. High-order ESVM

As is well-known, it is quite challenging for Lawson RK methods or prediction-correction Lawson RK methods to conserve general invariants. To address this issue, we choose to introduce a class of high-order ESVM methods by applying prediction-correction strategy to system (2.4). The essence lies in how to effectively determine the complementary parameter vector $\boldsymbol{\alpha} = (\alpha_1, \alpha_2) \in \mathbb{R}^2$ and guarantee the accuracy at the same time on both the semi and full-discrete level.

Scheme 3.2 (ESVM Scheme)**.** Let b_i, a_{ij} $(i, j = 1, \dots, s)$ be real numbers and $c_i = \sum_{j=1}^{s} a_{ij}$. Starting from a given z^n, we compute z^{n+1} in two steps.

- **High-order prediction:** let $z_{ni}^{(0)} = \exp(c_i\tau\mathcal{L})z^n$, compute $z_{ni}^{(\ell+1)}$ iteratively as

$$z_{ni}^{(\ell+1)} = \exp(c_i\tau\mathcal{L})z^n + \tau\sum_{j=1}^{s} a_{ij}\exp\big((c_i-c_j)\tau\mathcal{L}\big)\mathcal{N}[z_{nj}^{(\ell)}], \quad \ell = 0, \dots, M-1.$$

- **High-order correction:** update z^{n+1} as follows

$$\begin{cases} k_i = \mathcal{N}[z_{ni}^{(M)}] + \alpha_1^n g_1[z_{ni}^{(M)}] + \alpha_2^n g_2[z_{ni}^{(M)}], \\ z^{n+1} = \exp(\tau\mathcal{L})z^n + \tau\sum_{i=1}^{s} b_i\exp\big((1-c_i)\tau\mathcal{L}\big)\ k_i, \end{cases} \tag{3.4}$$

with suitable parameters α_1^n, α_2^n such that the energy and mass conservations

$$\mathcal{E}[z^{n+1}] = \mathcal{E}[z^n], \quad \mathcal{M}[z^{n+1}] = \mathcal{M}[z^n], \tag{3.5}$$

hold true at t_{n+1}.

Note that ESVM framework allows for a novel class of efficient exponential energy-preserving algorithms. In the following, we discuss the strategy on how to implement it efficiently. Firstly, Eq. (3.4) is rewritten as

$$z^{n+1} = \hat{z}^{n+1} + \beta_1\gamma_1^n + \beta_2\gamma_2^n, \quad \beta_1 = \tau\alpha_1^n, \quad \beta_2 = \tau\alpha_2^n, \tag{3.6}$$

with $\hat{z}^{n+1} = \exp(\tau\mathcal{L})z^n + \tau\sum_{i=1}^{s} b_i \exp\big((1-c_i)\tau\mathcal{L}\big)\mathcal{N}[z_{ni}^{(M)}]$ and

$$\gamma_j^n = \sum_{i=1}^{s} b_i \exp\big((1-c_i)\tau\mathcal{L}\big) g_j[z_{ni}^{(M)}], \quad j = 1, 2.$$

Inserting (3.6) into Eq. (3.5), we have

$$F_1(\tau, \boldsymbol{\beta}) := \mathcal{E}[\hat{z}^{n+1} + \beta_1\gamma_1^n + \beta_2\gamma_2^n] - \mathcal{E}[z^n] = 0, \tag{3.7}$$

$$F_2(\tau, \boldsymbol{\beta}) := \mathcal{M}[\hat{z}^{n+1} + \beta_1\gamma_1^n + \beta_2\gamma_2^n] - \mathcal{M}[z^n] = 0, \tag{3.8}$$

where $\boldsymbol{\beta} = (\beta_1, \beta_2)^\top$ and $\mathbf{F}(\tau, \boldsymbol{\beta}) = (F_1(\tau, \boldsymbol{\beta}), F_2(\tau, \boldsymbol{\beta}))^\top$. Instead of solving the fully implicit RK scheme for the unknown function $z^{n+1}(\mathbf{x})$, the algebraic equation of variable $\boldsymbol{\beta}$ is much cheaper to solve and can be computed efficiently via Newton iteration by taking $\mathbf{0}$ as the initial guess for $\boldsymbol{\beta}$. The specific Newton iteration scheme reads

$$\boldsymbol{\beta}^{(\ell+1)} = \boldsymbol{\beta}^{(\ell)} - [(J_{\boldsymbol{\beta}}\mathbf{F})(\tau, \boldsymbol{\beta}^{(\ell)})]^{-1}\mathbf{F}(\tau, \boldsymbol{\beta}^{(\ell)}), \quad \boldsymbol{\beta}^{(0)} = \mathbf{0}, \ \ell = 0, 1, \dots,$$

where the Jacobian is given explicitly

$$(J_{\boldsymbol{\beta}}\mathbf{F})(\tau, \boldsymbol{\beta}) := \begin{pmatrix} \frac{\partial F_1}{\partial \beta_1}(\tau, \boldsymbol{\beta}) & \frac{\partial F_1}{\partial \beta_2}(\tau, \boldsymbol{\beta}) \\ \frac{\partial F_2}{\partial \beta_1}(\tau, \boldsymbol{\beta}) & \frac{\partial F_2}{\partial \beta_2}(\tau, \boldsymbol{\beta}) \end{pmatrix}.$$

Inspired by ideas proposed in Hong et al. [2], Calvo et al. [33], we investigate the existence and uniqueness of $\boldsymbol{\beta}$ in Eqs. (3.7) and (3.8), and analyze the convergence order in local truncation error.

Theorem 4 (Local existence and uniqueness of $\boldsymbol{\beta}$). *If the Jacobian $(J_{\boldsymbol{\beta}}\mathbf{F})(0, \mathbf{0})$ is nonsingular, there exists a $\tau^* > 0$ such that the algebraic Eqs. (3.7) and (3.8) define a unique function $\boldsymbol{\beta} = \boldsymbol{\beta}(\tau)$ for all $\tau \in [0, \tau^*]$.*

Proof. Considering the smoothness of $\mathbf{F}(\tau, \boldsymbol{\beta})$ and condition

$$\mathbf{F}(0, \mathbf{0}) = \mathbf{0}, \quad \Big|(J_{\boldsymbol{\beta}}\mathbf{F})(0, \mathbf{0})\Big| \neq 0,$$

using the implicit function theorem, there exists a $\tau^* > 0$ such that the equation system $\mathbf{F}(\tau, \boldsymbol{\beta}) = \mathbf{0}$ defines a unique smooth function $\boldsymbol{\beta} = \boldsymbol{\beta}(\tau)$ satisfying $\boldsymbol{\beta}(\mathbf{0}) = \mathbf{0}$ and $\mathbf{F}(\tau, \boldsymbol{\beta}(\tau)) = \mathbf{0}$ for all $\tau \in [0, \tau^*]$. □

Remark 3. It is not difficult to check that

$$(J_{\boldsymbol{\beta}}\mathbf{F})(0, \mathbf{0}) = \begin{pmatrix} 2\Re\Big(g_1[z^n], \frac{\delta\mathcal{E}}{\delta z^*}[z^n]\Big) & 2\Re\Big(g_2[z^n], \frac{\delta\mathcal{E}}{\delta z^*}[z^n]\Big) \\ 2\Re\Big(g_1[z^n], \frac{\delta\mathcal{M}}{\delta z^*}[z^n]\Big) & 2\Re\Big(g_2[z^n], \frac{\delta\mathcal{M}}{\delta z^*}[z^n]\Big) \end{pmatrix} = 2J[z^n].$$

This indicates that the condition for the existence and uniqueness of solution in discrete scenario remains consistent with that in continuous context.

Remark 4. It is worthy to point out that Cheng, Shen and Wang [34] presented unique solvability and a detailed error analysis of Lagrange multiplier scheme for gradient flows. While, due to the multiple supplementary variables and Lawson Runge–Kutta method, a complete and detailed error analysis of ESVM is somehow challenging and technically involved, and we shall report it in a future article.

Theorem 5 (Convergence order in local truncation error). *If the underlying RK method is of order p and $|(J_{\boldsymbol{\beta}}\mathbf{F})(0, \boldsymbol{0})| \neq 0$, then the ESVM Scheme 3.2 is of order $\hat{p}$, where $\hat{p} = \min\{p, M+1\}$.*

Proof. We note that $\hat{z}^{n+1}$ satisfies

$$\hat{z}^{n+1} = \exp(\tau\mathcal{L})z^n + \tau\sum_{i=1}^{s} b_i \exp\big((1-c_i)\tau\mathcal{L}\big)\mathcal{N}[z_{ni}^{(M)}]. \tag{3.9}$$

According to the local truncation error analysis and using Theorems 2 and 3, we have

$$\hat{z}^{n+1} = z(t_{n+1}) + \mathcal{O}(\tau^{\min\{p, M+1\}+1}). \tag{3.10}$$

By the Taylor expansion, we then obtain

$$\mathcal{E}[\hat{z}^{n+1}] = \mathcal{E}[z(t_{n+1})] + \mathcal{O}(\tau^{\min\{p, M+1\}+1}),$$

and

$$\mathcal{M}[\hat{z}^{n+1}] = \mathcal{M}[z(t_{n+1})] + \mathcal{O}(\tau^{\min\{p, M+1\}+1}).$$

Since $z(t_{n+1})$ is the local solution of (2.1), it satisfies

$$z(t_n) = z^n, \ \mathcal{E}[z(t_{n+1})] = \mathcal{E}[z^n], \ \mathcal{M}[z(t_{n+1})] = \mathcal{M}[z^n].$$

Thus, we have

$$\mathcal{E}[\hat{z}^{n+1}] - \mathcal{E}[z^n] = \mathcal{O}(\tau^{\min\{p, M+1\}+1}), \ \mathcal{M}[\hat{z}^{n+1}] - \mathcal{M}[z^n] = \mathcal{O}(\tau^{\min\{p, M+1\}+1}).$$

Meanwhile, we expand $\mathbf{F}(\tau,\boldsymbol{\beta})$ at $\boldsymbol{\beta}=\mathbf{0}$ as

$$\mathbf{F}(\tau,\boldsymbol{\beta})=\mathbf{F}(\tau,\mathbf{0})+(J_{\boldsymbol{\beta}}\mathbf{F})(\tau,\mathbf{0})\boldsymbol{\beta}+\mathcal{O}(|\boldsymbol{\beta}|^2),$$

where

$$\mathbf{F}(\tau,\mathbf{0})=(\mathcal{E}[\hat{z}^{n+1}]-\mathcal{E}[z^n],\mathcal{M}[\hat{z}^{n+1}]-\mathcal{M}[z^n])^{\top}=\mathcal{O}(\tau^{\min\{p,M+1\}+1}),$$

$$(J_{\boldsymbol{\beta}}\mathbf{F})(\tau,\mathbf{0})=(J_{\boldsymbol{\beta}}\mathbf{F})(0,\mathbf{0})+\mathcal{O}(\tau).$$

This implies

$$\beta_1=\beta_1(\tau)=\mathcal{O}(\tau^{\hat{p}+1}),\ \beta_2=\beta_2(\tau)=\mathcal{O}(\tau^{\hat{p}+1}),\ \hat{p}=\min\{p,M+1\}. \tag{3.11}$$

Thus, using Eqs. (3.6) and (3.10) and (3.11), we have $z^{n+1}-z(t_{n+1})=\mathcal{O}(\tau^{\hat{p}+1})$. □

Remark 5 (Estimates on the magnitudes of supplementary variables α_1 and α_2)**.** According to Eq. (3.11), we obtain the following estimates

$$\alpha_i^n=\mathcal{O}(\tau^{\hat{p}}),\quad i=1,2, \tag{3.12}$$

which means both variables approach zero with the same integer order $\hat{p}$.

In fact, we can rewrite (3.12) as $\alpha_i^n=C_i(z^n)\tau^{\hat{p}}+\mathcal{O}(\tau^{\hat{p}+1})$. By assumption that $z^n=z(t_n)+\mathcal{O}(\tau)$ in the global error analysis, we then have

$$\alpha_i^n=C_i(z(t_n))\tau^{\hat{p}}+\mathcal{O}(\tau^{\hat{p}+1}), \tag{3.13}$$

which implies immediately that the convergence orders are both $\hat{p}$.

4. Numerical results

In this section, we begin with the classical single-component nonlinear GP Eq. (2.6) arising from the BEC simulation, and employ our mass- and energy-conserving ESVM schemes for it. Then, we present a series of numerical examples to measure the accuracy and efficiency of our proposed schemes, in comparison with existing structure-preserving numerical methods. Additionally, we extend the ESVM approach to multi-component GP equations. Finally, we present the mass- and energy-conserving ESVM schemes for the SP equation, and compare them with the SVM schemes.

4.1. Single-component GP equation

In this subsection, we employ the ESVM approach to solve the single-component GP Eq. (2.6), resulting in the following semi-discrete system

Scheme 4.1 (Semi-discrete ESVM Scheme)**.** Let b_i,a_{ij} $(i,j=1,\dots,s)$ be real numbers and $c_i=\sum_{j=1}^s a_{ij}$. From a given wave function ψ^n, we update ψ^{n+1} in two steps.

- **High-order prediction:** let $\psi_{ni}^{(0)}=\exp(c_i\tau\frac{\mathrm{i}}{2}\Delta)\psi^n$, compute $\psi_{ni}^{(\ell+1)},\ \ell=0,\dots,M-1$ iteratively as

$$\begin{cases}\psi_{ni}^{(\ell+1)}=\exp(c_i\tau\frac{\mathrm{i}}{2}\Delta)\psi^n+\tau\sum\limits_{j=1}^{s}a_{ij}\exp((c_i-c_j)\tau\frac{\mathrm{i}}{2}\Delta)k_j^{(\ell+1)},\\ k_i^{(\ell+1)}=-\mathrm{i}\big(V(\mathbf{x})-\Omega L_z+\beta|\psi_{ni}^{(\ell)}|^2\big)\psi_{ni}^{(\ell)}.\end{cases} \tag{4.1}$$

- **High-order correction:** update ψ^{n+1} by

$$\begin{cases}k_i=-\mathrm{i}\big(V(\mathbf{x})-\Omega L_z+\beta|\psi_{ni}^{(M)}|^2\big)\psi_{ni}^{(M)}+\alpha_1^n g_1[\psi_{ni}^{(M)}]+\alpha_2^n g_2[\psi_{ni}^{(M)}],\\ g_1[\psi_{ni}^{(M)}]=\Big[\frac{1}{2}\Delta-V(\mathbf{x})+\Omega L_z-\beta|\psi_{ni}^{(M)}|^2\Big]\psi_{ni}^{(M)},\ g_2[\psi_{ni}^{(M)}]=\psi_{ni}^{(M)},\\ \psi^{n+1}=\exp(\tau\frac{\mathrm{i}}{2}\Delta)\psi^n+\tau\sum\limits_{i=1}^{s}b_i\exp((1-c_i)\tau\frac{\mathrm{i}}{2}\Delta)k_i,\end{cases} \tag{4.2}$$

with suitable parameters α_1^n,α_2^n such that the energy and mass conservations

$$\mathcal{E}[\psi^{n+1}]=\mathcal{E}[\psi^n],\ \mathcal{M}[\psi^{n+1}]=\mathcal{M}[\psi^n].$$

Due to presence of the external trapping potential, the wave function is usually smooth and decays exponentially fast at the far field. Therefore, it is reasonable to truncate the whole space into a bounded rectangular domain $\mathcal{D}=[-L,L]^2$, that is usually discretized uniformly in each spatial direction with the same mesh size $h=2L/N,\ N\in 2\mathbb{Z}^+$, and impose periodic boundary conditions. Then, we can readily apply the Fourier spectral method [35,39] to approximate the wave function and achieve spectral accuracy with a

nearly optimal efficiency of complexity $\mathcal{O}(N^2 \log N^2)$ thanks to discrete Fast Fourier transform (FFT). For simplicity, we define the physical index, Fourier index and grid points sets as

$$\mathcal{I}_N = \{(j,k) \in \mathbb{Z}^2 \Big| \ 0 \le j \le N-1, \quad 0 \le k \le N-1\},$$

$$\Lambda_N = \{(p,q) \in \mathbb{Z}^2 \Big| \ -(N/2-1) \le p, \ q \le N/2\},$$

$$\mathcal{G} = \{\mathbf{x}_{jk} := (x_j, y_k) \Big| x_j = -L + jh, \quad y_k = -L + kh, \quad (j,k) \in \mathcal{I}_N\},$$

and denote $\psi_{j,k}(t)$ as the numerical approximation of $\psi(\mathbf{x}_{jk}, t)$ for $\mathbf{x}_{jk} \in \mathcal{G}$. We then employ the Fourier spectral approximation in space for (4.1) and (4.2). To be specific, the spectral approximation of wave function ψ reads as follows

$$\psi(x,y) \approx \sum_{(p,q)\in\Lambda_N} \widehat{\psi}_{p,q} \ e^{\mathrm{i}v_p^x(x+L)} e^{\mathrm{i}v_q^y(y+L)},$$

and the Fourier coefficient is given by

$$\widehat{\psi}_{p,q} = \frac{1}{N^2} \sum_{(j,k)\in\mathcal{I}_N} \psi(\mathbf{x}_{jk}) e^{-\mathrm{i}v_p^x(x_j+L)} e^{-\mathrm{i}v_q^y(y_k+L)},$$

where $v_p^x = \pi p/L, \ v_q^y = \pi q/L$. The terms $\Delta\psi, \ y\partial_x\psi, \ x\partial_y\psi$ and $e^{t\mathcal{L}}\psi \ \left(\mathcal{L} = \frac{\mathrm{i}}{2}\Delta\right)$ are approximated as follows

$$\Delta\psi(\mathbf{x}_{jk}) \approx \sum_{(p,q)\in\Lambda_N} -\left[(v_p^x)^2 + (v_q^y)^2\right] \widehat{\psi}_{p,q} e^{\mathrm{i}v_p^x(x_j+L)} e^{\mathrm{i}v_q^y(y_k+L)}, \tag{4.3}$$

$$(y\partial_x)\psi(\mathbf{x}_{jk}) \approx y_k \sum_{(p,q)\in\Lambda_N} (\mathrm{i}v_p^x) \ \widehat{\psi}_{p,q} \ e^{\mathrm{i}v_p^x(x_j+L)} \ e^{\mathrm{i}v_q^y(y_k+L)}, \tag{4.4}$$

$$(x\partial_y)\psi(\mathbf{x}_{jk}) \approx x_j \sum_{(p,q)\in\Lambda_N} (\mathrm{i}v_q^y) \ \widehat{\psi}_{p,q} \ e^{\mathrm{i}v_p^x(x_j+L)} \ e^{\mathrm{i}v_q^y(y_k+L)}, \tag{4.5}$$

$$(e^{t\mathcal{L}})\psi(\mathbf{x}_{jk}) \approx \sum_{(p,q)\in\Lambda_N} e^{-t\frac{\mathrm{i}}{2}\left[(v_p^x)^2+(v_q^y)^2\right]} \widehat{\psi}_{p,q} e^{\mathrm{i}v_p^x(x_j+L)} e^{\mathrm{i}v_q^y(y_k+L)}. \tag{4.6}$$

Remark 6. The approximation (4.6) implies that exponential operator $e^{t\mathcal{L}}$ can be efficiently implemented in the Fourier space. If homogeneous Dirichlet or Neumann boundary conditions are specified, we employ sine/cosine pseudo-spectral method [35] for spatial discretization, and the exponential operator $e^{t\mathcal{L}}$ is computed efficiently by combining the matrix diagonalization method with the discrete sine/cosine transform.

In this study, we consider two ESVM schemes—specifically, the second-order (ESVM2) and fourth-order (ESVM4) versions—for demonstration purposes. To evaluate their performance, these are compared against several benchmark methods of matching orders: the SVM2/SVM4 schemes [2], Gauss2/Gauss4 integrators [6], Besse–Dujardin–Lacroix exponential integrators (BDL2/BDL4) [30], and the Crank–Nicolson (CN2) method [28].

To quantify the numerical errors, we denote the numerical approximation of $\psi(\cdot, t_n)$ as $\psi_{\tau,h}^n$, which is obtained with mesh size h and time step τ, and define the discrete l^2-error and convergence order as

$$e_2^{\tau,h}(t_n) = \|\psi(\cdot,t_n) - \psi_{\tau,h}^n\|_{l^2}, \quad \text{Order} = \ln\left(e_2^{\tau_1,h}(t_n)/e_2^{\tau_2,h}(t_n)\right)/\ln(\tau_1/\tau_2).$$

The errors of mass and energy are measured as follows

$$e_{\mathcal{M}}(t_n) = |\mathcal{M}^n - \mathcal{M}^0|/|\mathcal{M}^0|, \qquad e_{\mathcal{E}}(t_n) = |\mathcal{E}^n - \mathcal{E}^0|/|\mathcal{E}^0|.$$

In the following, we shall consider the rotating GP Eq. (2.6) with

$$\Omega = 0.9, \ \beta = 100, \ \gamma_x = \gamma_y = 1, \tag{4.7}$$

and the initial condition

$$\psi(\mathbf{x},0) = \frac{2}{\sqrt{\pi}}(x + \mathrm{i}y)\exp\left(-(x^2+y^2)\right). \tag{4.8}$$

To compute the aforementioned equation in practice, we choose $M = 2$ for the ESVM2/SVM2 schemes and $M = 4$ for the ESVM4/SVM4 schemes. The fixed-point iteration is employed to solve the fully-implicit schemes with a very strict convergence tolerance 10^{-14}. In the accuracy confirmation and efficiency performance investigation, all numerical errors are calculated using $N = 128^2$ on $D = [-16, 16]^2$ such that the errors coming from spatial discretization are negligible. All simulations are run using MATLAB R2015b on a Win10 machine with Intel Core i7-9700 and 32 GB memory.

Example 1 (Accuracy confirmation). In this example, we compare the accuracy performance of different methods in the temporal direction. The reference solution is obtained by ESVM4 with a very small time step $\tau = 10^{-4}$.

Table 2
Temporal accuracy and convergence at $T = 1$ in Example 1[a].

Second-order scheme					
		$\tau_0 = 1/260$	$\tau_0/2$	$\tau_0/4$	$\tau_0/8$
ESVM2	$e_2^{\tau,h}(T=1)$	2.862E−03	7.117E−04	1.776E−04	4.439E−05
	Order	–	2.008	2.002	2.001
SVM2	$e_2^{\tau,h}(T=1)$	*	4.625E−03	1.158E−03	2.896E−04
	Order	–	–	1.998	2.000
BDL2	$e_2^{\tau,h}(T=1)$	2.729E−03	6.837E−04	1.710E−04	4.276E−05
	Order	–	1.997	1.999	2.000
Gauss2	$e_2^{\tau,h}(T=1)$	1.808E−02	4.595E−03	1.152E−03	2.881E−04
	Order	–	1.976	1.996	1.999
CN2	$e_2^{\tau,h}(T=1)$	1.665E−02	4.228E−03	1.059E−03	2.649E−04
	Order	–	1.977	1.997	1.999
Fourth-order scheme					
		$\tau_0 = 1/170$	$\tau_0/2$	$\tau_0/4$	$\tau_0/8$
ESVM4	$e_2^{\tau,h}(T=1)$	3.782E−06	2.130E−07	1.315E−08	8.191E−10
	Order	–	4.150	4.018	4.005
SVM4	$e_2^{\tau,h}(T=1)$	*	6.980E−06	4.376E−07	2.737E−8
	Order	–	–	3.996	3.999
BDL4	$e_2^{\tau,h}(T=1)$	3.275E−06	2.061E−07	1.290E−08	8.066E−10
	Order	–	3.990	3.998	4.000
Gauss4	$e_2^{\tau,h}(T=1)$	1.101E−04	6.976E−06	4.375E−07	2.737E−08
	Order	–	3.980	3.995	3.999

[a] Here $*$ represents numerical divergence of the iteration procedure for solving the nonlinear equation.

Table 3
Temporal accuracy and convergence at $T = 20$ in Example 1.

Second-order scheme					
		$\tau_0 = 1/260$	$\tau_0/2$	$\tau_0/4$	$\tau_0/8$
ESVM2	$e_2^{\tau,h}(T=20)$	9.379E−02	2.706E−02	7.215E−03	1.812E−03
	Order	–	1.794	1.907	1.993
SVM2	$e_2^{\tau,h}(T=20)$	*	6.567E−02	1.957E−02	5.100E−03
	Order	–	–	1.747	1.940
BDL2	$e_2^{\tau,h}(T=20)$	8.952E−02	2.616E−02	7.017E−03	1.766E−03
	Order	–	1.775	1.898	1.990
Gauss2	$e_2^{\tau,h}(T=20)$	2.190E−01	6.459E−02	1.934E−02	5.049E−03
	Order	–	1.762	1.740	1.938
CN2	$e_2^{\tau,h}(T=20)$	1.966E−01	5.889E−02	1.812E−02	4.753E−03
	Order	–	1.739	1.701	1.931
Fourth-order scheme					
		$\tau_0 = 1/180$	$\tau_0/2$	$\tau_0/4$	$\tau_0/8$
ESVM4	$e_2^{\tau,h}(T=20)$	6.901E−04	4.005E−05	2.449E−06	1.522E−07
	Order	–	4.107	4.031	4.009
SVM4	$e_2^{\tau,h}(T=20)$	*	1.496E−04	9.322E−06	5.821E−07
	Order	–	–	4.004	4.001
BDL4	$e_2^{\tau,h}(T=20)$	6.106E−04	3.871E−05	2.428E−06	1.518E−07
	Order	–	3.980	3.995	3.999
Gauss4	$e_2^{\tau,h}(T=20)$	2.303E−03	1.482E−04	9.298E−06	5.816E−07
	Order	–	3.958	3.994	3.999

Temporal errors and convergence orders are displayed in Tables 2 and 3, from which one can observe the following: (i) ESVM2, SVM2, BDL2, Gauss2 and CN2 are all second-order in time, while ESVM4, SVM4, BDL4 and Gauss4 are fourth-order. (ii) Exponential methods are more accurate than the other classical ones when compared in terms of the error magnitudes. (iii) High-order schemes produce much more accurate solutions and the ESVM schemes are more robust than SVM schemes. To be more specific, SVM2 diverges at a larger time step $\tau_0 = 1/260$ for $T = 1$ and $T = 20$, and SVM4 diverges at a larger time steps $\tau_0 = 1/170$ and $\tau_0 = 1/180$ for $T = 1$ and $T = 20$, respectively.

Furthermore, Fig. 1 illustrates the maximum allowable time steps for various numerical schemes as functions of the final time T. Specifically, any step size exceeding these thresholds causes solution divergence or numerical instability. As evident from the plot,

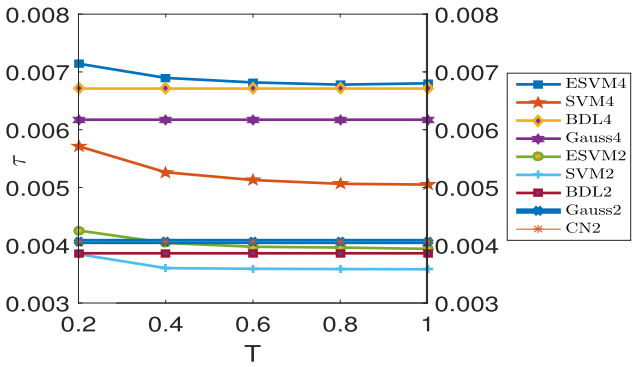

Fig. 1. Maximum time steps versus time T in Example 1.

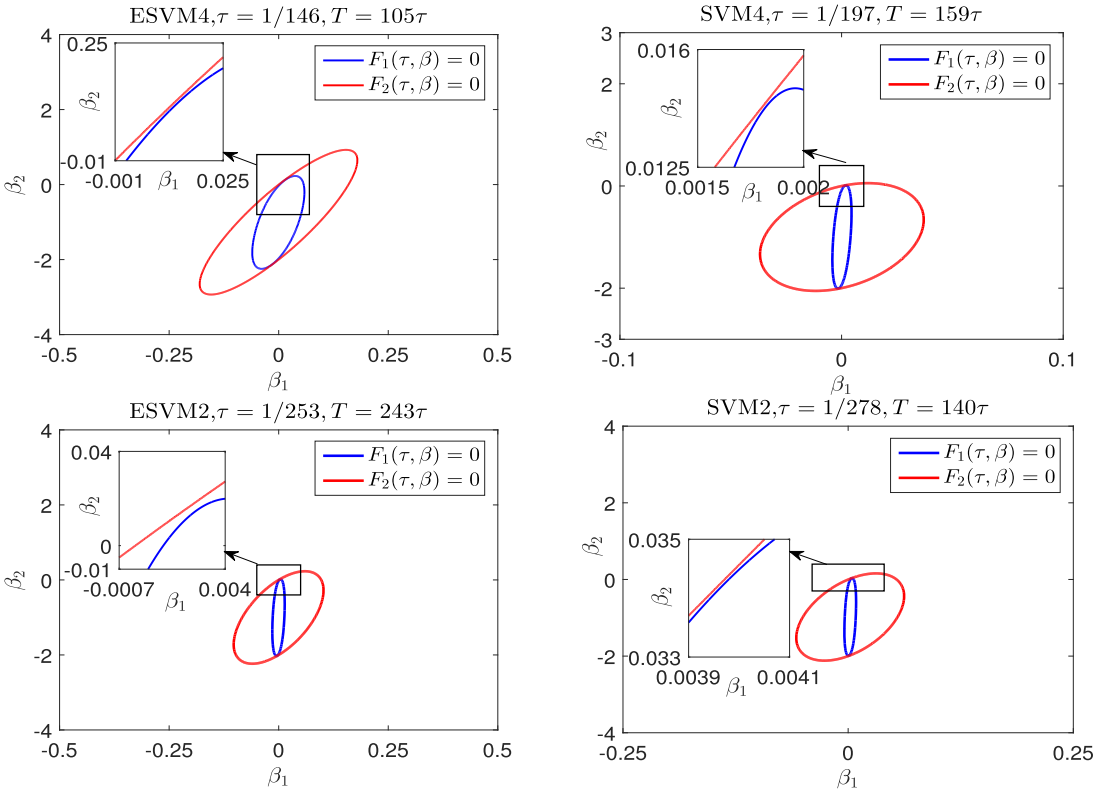

Fig. 2. The curves of $F_1(\tau,\boldsymbol{\beta})=0$ & $F_2(\tau,\boldsymbol{\beta})=0$ for the ESVM & SVM schemes in Example 1.

ESVM4 permits significantly larger time steps than SVM4, BDL4, and Gauss4; similarly, ESVM2 supports substantially larger steps than both SVM2 and BDL2. In fact, whether the algebraic system defined by (3.7) and (3.8) has real roots plays a critical role in determining the applicability of both ESVM and SVM schemes. Fig. 2 demonstrates that when time steps surpass their respective maxima, the zero contours of (3.7) and (3.8) fail to intersect at the origin $(0,0)$.

To compare the accuracy performance with other existing methods, we present in Fig. 3 the numerical errors of the wave function at time $T=1$ obtained using different time steps. The results show that the ESVM schemes can achieve the desired accuracy even with larger time steps. Moreover, compared to the SVM methods, ESVM schemes demonstrate superior numerical stability.

Finally, Fig. 4 displays the evolution and convergence orders of the supplementary variables α_1^n and α_2^n for the ESVM2 and ESVM4 schemes. The plotted results confirm two key points: (i) these variables remain consistently close to zero, and (ii) ESVM2 exhibits second-order accuracy in time, whereas ESVM4 achieves fourth-order accuracy in time. These findings are in excellent agreement with the theoretical predictions made in Remark 5.

Example 2 (Computational efficiency). In this example, we compare the computational efficiency of different numerical schemes by investigating the dependence of accuracy variation on CPU time elapsed (measured in seconds).

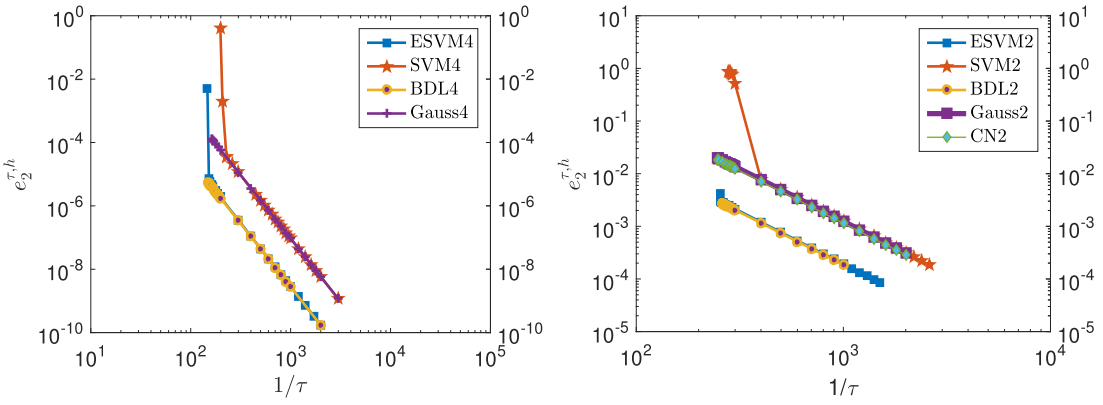

Fig. 3. Accuracy versus time steps at $T = 1$ in Example 1.

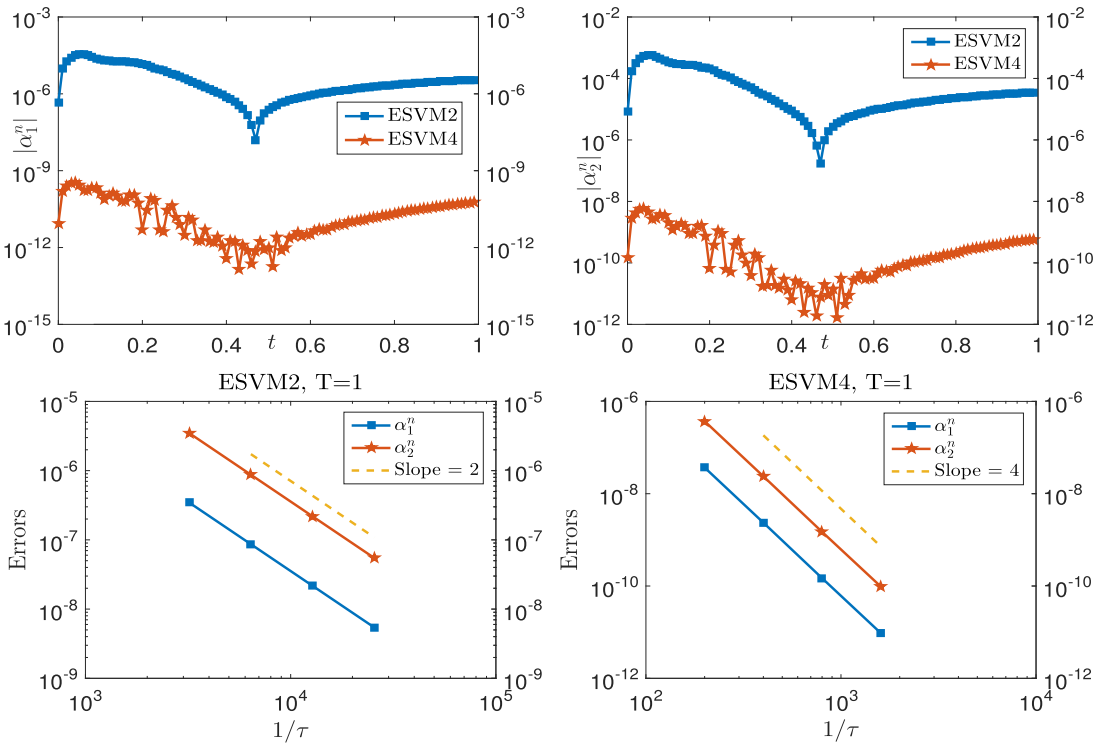

Fig. 4. The evolution (top row) and convergence order (bottom row) of the supplementary variables α_1^n & α_2^n for the ESVM2 & ESVM4 schemes in Example 1.

Fig. 5 shows the errors $e_2^{\tau,h}$ plotted against computational time elapsed. It is evident that ESVM requires the least CPU time among all compared methods for any given precision. For example, targeting an error around 1.7×10^{-6}, the CPU times needed by ESVM2, SVM2, BDL2, Gauss2, and CN2 are 809, 1919, 756, 1111 and 1160 seconds, respectively. Meanwhile, the fourth-order variants (ESVM4, SVM4, BDL4, Gauss4) demand substantially less computation time: 39, 93, 285 and 184 seconds, respectively.

Example 3 (Long-time evolution of conservation laws). In this example, we investigate the preservation of two conserved quantities: mass and energy. We first show the variation of numerical errors $e_{\mathcal{M}}$ and $e_{\mathcal{E}}$ for different time steps τ, then present the long-time evolution for different numerical schemes where the time t reaches as large as 10^3. To this end, the wave functions are computed with mesh grid $N = 64^2$ on domain $D = [-20, 20]^2$.

Fig. 6 shows the preservation of mass and energy versus different time steps τ, while the long-time evolution is displayed in Fig. 7. From these figures, we draw the following conclusions: (i) All numerical schemes conserve mass, with SVM and ESVM demonstrating significantly lower error magnitudes and superior roundoff stability compared to other methods. (ii) Only SVM, ESVM and CN2 conserve the original energy. Notably, the energy error of CN2, whose magnitude strongly depends on the accuracy of fixed-point

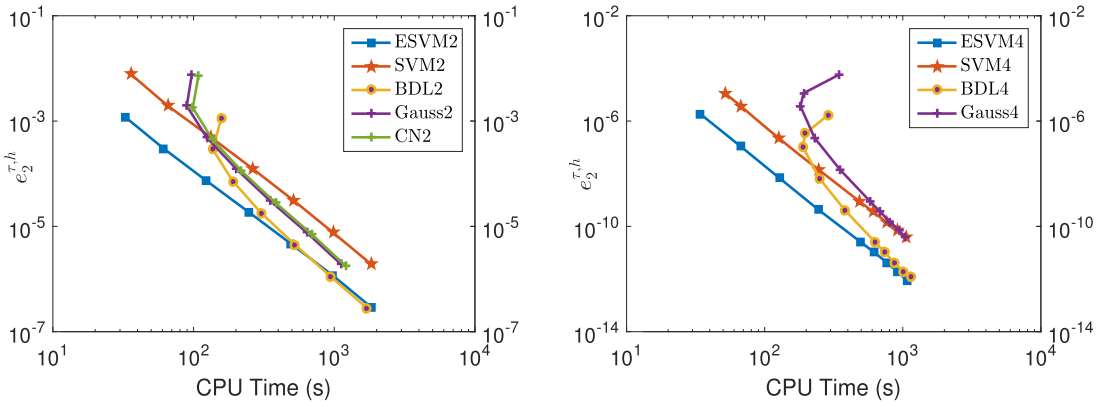

Fig. 5. Accuracies versus CPU times for Eq. (2.6) in Example 2.

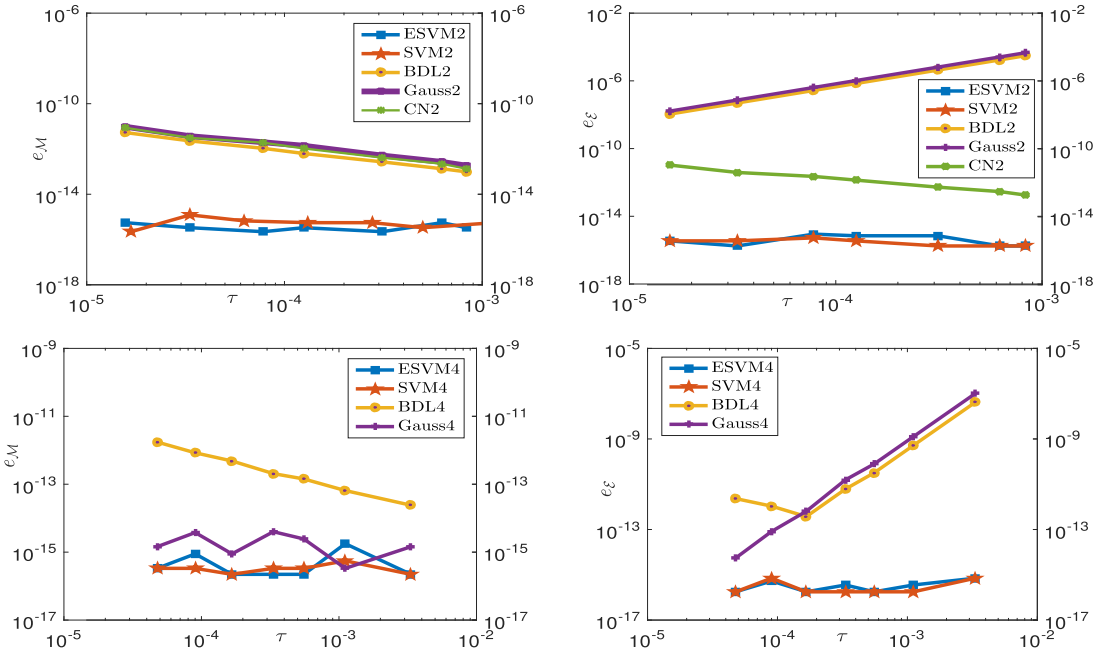

Fig. 6. Preservation of mass (left) and energy (right) for different time steps in Example 3.

iterations used to solve nonlinear equations, is at least three orders of magnitude larger than that of SVM/ESVM. (iii) In long-time simulations, SVM and ESVM exhibit exceptional superiority in preserving both mass and energy. Surprisingly, a linear increase in mass and energy errors occurs for CN2 as the simulation progresses, likely due to accumulated fixed-point iteration errors and roundoff propagation. For all other schemes, both $e_{\mathcal{M}}$ and $e_{\mathcal{E}}$ show the expected growth over time.

Example 4 (Applications to BEC). In this example, we apply the ESVM4 scheme to simulate the dynamics of GP equation. For the rotating GP Eqs. (2.6) and (2.7), the initial wave function is obtained by computing the ground state using the preconditioned conjugate gradient method [36,37], with parameters set to $\beta = 100$, $\Omega = 0.93$ and $\gamma_x = \gamma_y = 1$. Subsequently, we evolve the system under modified parameters: $\beta = 100$, $\Omega = 0.93$, $\gamma_x = 1.5$, $\gamma_y = 1$, utilizing a spatial discretization of $N = 896$ and time step $\tau = 1/4000$ on the two-dimensional domain $D = [-14, 14]^2$.

Fig. 8 illustrates the contour plots of the density function $\rho(\mathbf{x}, t) := |\psi(\mathbf{x}, t)|^2$ at different times and the relative errors of mass and energy, from which we can see that our scheme conserves the mass and energy very well with errors approaching machine-precision.

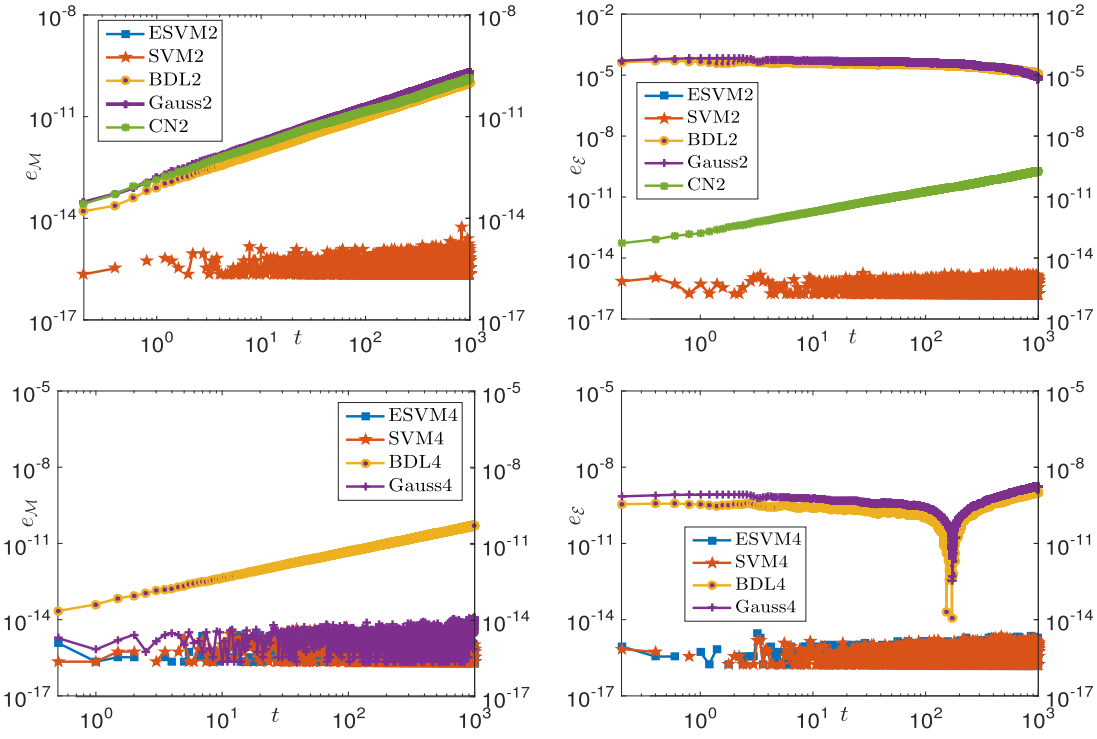

Fig. 7. Long-time evolution of $e_{\mathcal{M}}$ & $e_{\mathcal{E}}$ for solutions obtained with very small time step $\tau = 10^{-3}$ in Example 3.

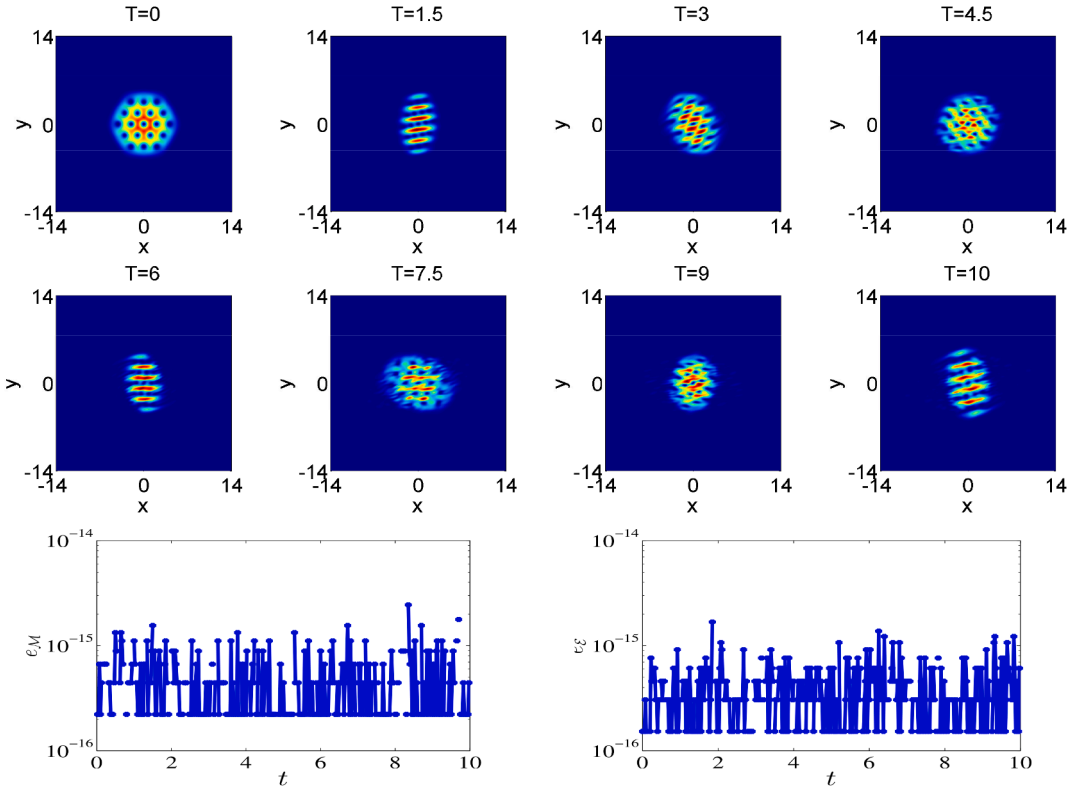

Fig. 8. The density function $\rho := |\psi(\mathbf{x}, t)|^2$ (top row) and mass & energy errors (bottom row)) in Example 4.

4.2. Applications to multi-component GP equations

In this subsection, we extend the ESVM approach to multi-component GP equations (mGPE), as described by

$$\begin{cases} \mathrm{i}\dfrac{\partial}{\partial t}\psi_1 = \Big(-\dfrac{1}{2}\Delta + V_1(\mathbf{x}) - \Omega L_z + \displaystyle\sum_{l=1}^{2}\beta_{1l}|\psi_l|^2\Big)\psi_1 - \lambda\psi_2, \\ \mathrm{i}\dfrac{\partial}{\partial t}\psi_2 = \Big(-\dfrac{1}{2}\Delta + V_2(\mathbf{x}) - \Omega L_z + \displaystyle\sum_{l=1}^{2}\beta_{2l}|\psi_l|^2\Big)\psi_2 - \lambda\psi_1, \\ \psi_1(\mathbf{x},0) = \psi_1^0(\mathbf{x}),\ \ \psi_2(\mathbf{x},0) = \psi_2^0(\mathbf{x}), \end{cases} \tag{4.9}$$

where $\psi_1(\mathbf{x},t), \psi_2(\mathbf{x},t)$ are complex-valued wave functions, β_{1l} and β_{2l} are local interaction strength, and $\psi_1^0(\mathbf{x})$ and $\psi_2^0(\mathbf{x})$ are the initial profiles. The external potential is taken as

$$V_j(\mathbf{x}) = \frac{1}{2}\Big(\gamma_{x,j}^2 x^2 + \gamma_{y,j}^2 y^2\Big), \quad j = 1, 2, \tag{4.10}$$

with $\gamma_{x,j} > 0, \gamma_{y,j} > 0$ being the trapping frequencies in x and y direction respectively.

Denoting $z = \big[\psi_1, \psi_2\big]^{\top}$, the mGPE (4.9) is reformulated into

$$\partial_t z = \mathcal{L}z + \mathcal{N}[z],$$

with

$$\mathcal{L} = \begin{bmatrix} \frac{\mathrm{i}}{2}\Delta & \mathrm{i}\lambda \\ \mathrm{i}\lambda & \frac{\mathrm{i}}{2}\Delta \end{bmatrix}, \quad \mathcal{N}[z] = \begin{bmatrix} -\mathrm{i}\big(V_1(\mathbf{x}) - \Omega L_z + \sum_{l=1}^{2}\beta_{1l}|\psi_l|^2\big)\psi_1 \\ -\mathrm{i}\big(V_2(\mathbf{x}) - \Omega L_z + \sum_{l=1}^{2}\beta_{2l}|\psi_l|^2\big)\psi_2 \end{bmatrix}.$$

The mGPE system (4.9) conserves both the energy

$$\mathcal{E}[z] = \int_{\mathbb{R}^2}\sum_{j=1}^{2}\left[-\frac{1}{2}|\nabla\psi_j|^2 - V_j|\psi_j|^2 + \Omega\psi_j^* L_z\psi_j - \frac{1}{2}\sum_{l=1}^{2}\beta_{jl}|\psi_l|^2|\psi_j|^2\right] + \lambda(\psi_1^*\psi_2 + \psi_2^*\psi_1)\mathrm{d}\mathbf{x},$$

and the total mass $\mathcal{M}[z] := \sum_{j=1}^{2}\int_{\mathbb{R}^2}|\psi_j(\mathbf{x},t)|^2\mathrm{d}\mathbf{x}$.

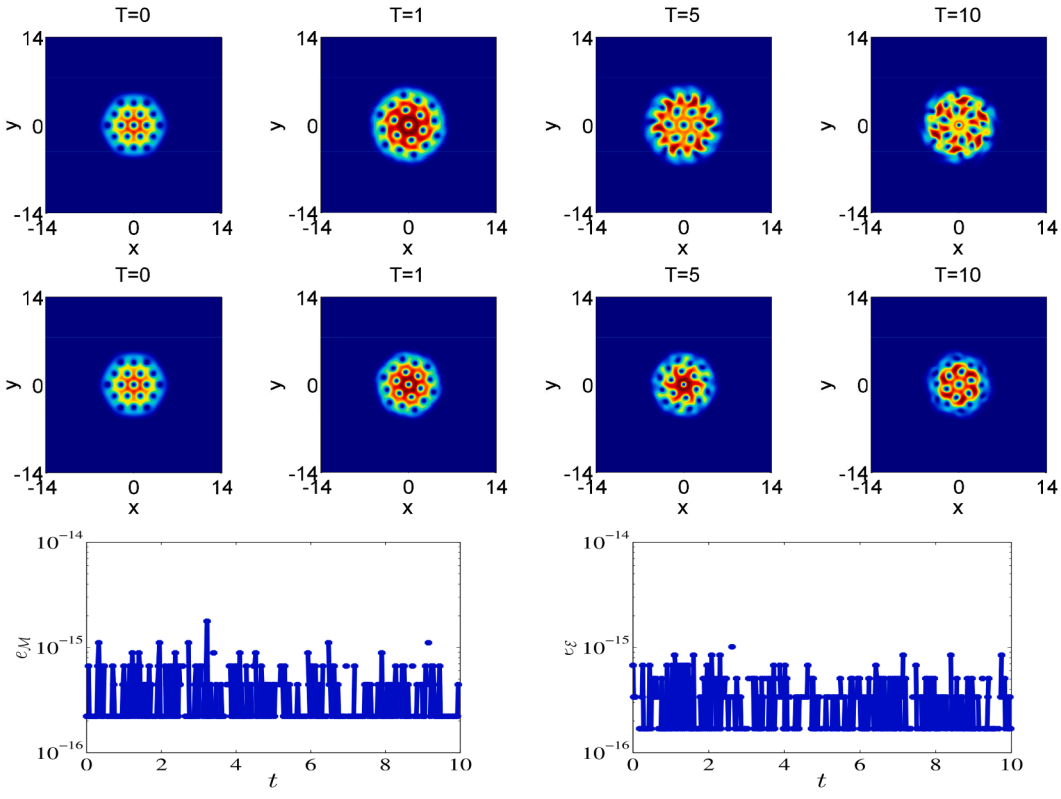

Fig. 9. The density functions $|\psi_1(\mathbf{x},t)|^2$ (top row) & $|\psi_2(\mathbf{x},t)|^2$ (middle row) and mass & energy errors (bottom row) in Example 5.

Following a similar procedure as proposed in Section 2, the ESVM reformulation of Eq. (4.9) is

$$\begin{cases} \partial_t Z = \exp(-\mathcal{L}t)\mathcal{N}[z] + \alpha_1 \exp(-\mathcal{L}t) g_1[z] + \alpha_2 \exp(-\mathcal{L}t) g_2[z], \ z = \exp(\mathcal{L}t) Z, \\ \dfrac{d}{dt}\mathcal{E}[z] = 0, \ \dfrac{d}{dt}\mathcal{M}[z] = 0, \end{cases} \tag{4.11}$$

where

$$g_1[z] = \begin{bmatrix} (\frac{1}{2}\Delta - V_1(\mathbf{x}) + \Omega L_z - \sum_{l=1}^{2} \beta_{1l}|\psi_l|^2)\psi_1 + \lambda\psi_2 \\ (\frac{1}{2}\Delta - V_2(\mathbf{x}) + \Omega L_z - \sum_{l=1}^{2} \beta_{2l}|\psi_l|^2)\psi_2 + \lambda\psi_1 \end{bmatrix}, \quad g_2[z] = \frac{\delta \mathcal{M}}{\delta z^*} = \begin{bmatrix} \psi_1 \\ \psi_2 \end{bmatrix}.$$

Remark 7. Noticing that

$$\mathcal{L} = \mathcal{P}^{\top} \Lambda \mathcal{P}, \quad \mathcal{P} = \frac{1}{\sqrt{2}} \begin{bmatrix} 1 & 1 \\ 1 & -1 \end{bmatrix}, \quad \Lambda = \begin{bmatrix} \frac{\mathrm{i}}{2}\Delta + \mathrm{i}\lambda & 0 \\ 0 & \frac{\mathrm{i}}{2}\Delta - \mathrm{i}\lambda \end{bmatrix},$$

we then have

$$\begin{aligned} \exp(t\mathcal{L}) &= \frac{1}{2}\begin{bmatrix} 1 & 1 \\ 1 & -1 \end{bmatrix} \begin{bmatrix} \exp(t\frac{\mathrm{i}}{2}\Delta + t\mathrm{i}\lambda) & 0 \\ 0 & \exp(t\frac{\mathrm{i}}{2}\Delta - t\mathrm{i}\lambda) \end{bmatrix} \begin{bmatrix} 1 & 1 \\ 1 & -1 \end{bmatrix} \\ &= \begin{bmatrix} \exp(t\frac{\mathrm{i}}{2}\Delta)\cos(t\lambda) & \mathrm{i}\exp(t\frac{\mathrm{i}}{2}\Delta)\sin(t\lambda) \\ \mathrm{i}\exp(t\frac{\mathrm{i}}{2}\Delta)\sin(t\lambda) & \exp(t\frac{\mathrm{i}}{2}\Delta)\cos(t\lambda) \end{bmatrix}. \end{aligned}$$

It is easy to see that the action of operator $e^{t\mathcal{L}}$ on fast-decaying smooth vector-valued functions can be implemented accurately and efficiently by Fourier spectral method together with the discrete Fast Fourier Transform (FFT).

Example 5 (Applications in multi-component BECs). In this example, we focus on the dynamics of mGPE (4.9). For the rotating mGPE (4.9) with the potential function (4.10), the initial wave functions are chosen as the ground state computed numerically using the preconditioned conjugated gradient method with parameters $\beta = 100$, $\Omega = 0.93$ and $\gamma_x = \gamma_y = 1$ in Eq. (2.6). In practice, we take $L = 14$, $N = 896$ and $\tau = \frac{1}{2000}$, and apply ESVM4 to simulate dynamics of mGPE (4.9) with parameters $\beta_{11} = \beta_{22} = 200$, $\beta_{12} = \beta_{21} = 100$, $\Omega = 0.9$, $\gamma_{x,1} = \gamma_{y,1} = 0.9$, $\gamma_{x,2} = \gamma_{y,2} = 1.1$ and $\lambda = 0$.

Fig. 9 shows the contour plots of the density functions $|\psi_1(\mathbf{x}, t)|^2$ (top row) & $|\psi_2(\mathbf{x}, t)|^2$ (middle row) at different times, and mass & energy errors (bottom row), from which we can observe clearly that the mass and energy are both preserved quite accurate around machine-precision.

4.3. ESVM scheme for the SP equation

In this subsection, we employ the ESVM approach to solve the SP Eq. (2.12), and the corresponding semi-discrete ESVM scheme is given by

Scheme 4.2 (Semi-discrete ESVM Scheme). Let b_i, a_{ij} $(i, j = 1, \dots, s)$ be real numbers and $c_i = \sum_{j=1}^{s} a_{ij}$. From a given wave function ψ^n, we update ψ^{n+1} in two steps.

- **High-order prediction:** let $\psi_{ni}^{(0)} = \exp(c_i \tau \frac{\mathrm{i}}{2}\Delta)\psi^n$, compute $\psi_{ni}^{(\ell+1)}$, $\ell = 0, \dots, M-1$ iteratively as

$$\begin{cases} \psi_{ni}^{(\ell+1)} = \exp(c_i \tau \dfrac{\mathrm{i}}{2}\Delta)\psi^n + \tau \displaystyle\sum_{j=1}^{s} a_{ij} \exp((c_i - c_j)\tau \frac{\mathrm{i}}{2}\Delta) k_i^{(\ell+1)}, \\ k_i^{(\ell+1)} = -\mathrm{i}\Big(V(\mathbf{x}) - \Omega L_z + \alpha \Phi_{ni}^{(\ell)}(|\psi_{ni}^{(\ell)}|^2) + \beta |\psi_{ni}^{(\ell)}|^2 \Big) \psi_{ni}^{(\ell)}. \end{cases}$$

- **High-order correction:** update ψ^{n+1} by

$$\begin{cases} k_i = -\mathrm{i}\Big(V(\mathbf{x}) - \Omega L_z + \alpha \Phi_{ni}^{(M)}(|\psi_{ni}^{(M)}|^2) + \beta |\psi_{ni}^{(M)}|^2 \Big) \psi_{ni}^{(M)} + \alpha_1^n g_1[\psi_{ni}^{(M)}] + \alpha_2^n g_2[\psi_{ni}^{(M)}], \\ g_1[\psi_{ni}^{(M)}] = \Big(\dfrac{1}{2}\Delta - V(\mathbf{x}) + \Omega L_z - \alpha \Phi_{ni}^{(M)}(|\psi_{ni}^{(M)}|^2) - \beta |\psi_{ni}^{(M)}|^2 \Big) \psi_{ni}^{(M)}, \ g_2[\psi_{ni}^{(M)}] = \psi_{ni}^{(M)}, \\ \psi^{n+1} = \exp(\tau \dfrac{\mathrm{i}}{2}\Delta)\psi^n + \tau \displaystyle\sum_{i=1}^{s} b_i \exp((1 - c_i)\tau \frac{\mathrm{i}}{2}\Delta) k_i, \end{cases}$$

with suitable parameters α_1^n, α_2^n such that the energy and mass conservations

$$\mathcal{E}[\psi^{n+1}] = \mathcal{E}[\psi^n], \quad \mathcal{M}[\psi^{n+1}] = \mathcal{M}[\psi^n].$$

Table 4
Temporal accuracy and convergence rate of ESVM & SVM scheme at $T = 1$ and $T = 20$ in Example 6.

Final time $T = 1$					
		$\tau_0 = 1/290$	$\tau_0/2$	$\tau_0/4$	$\tau_0/8$
ESVM2	$e_2^{\tau,h}(T=1)$	1.139E−05	2.846E−06	7.115E−07	1.779E−07
	Order	–	2.000	2.000	2.000
SVM2	$e_2^{\tau,h}(T=1)$	*	1.141E−05	2.852E−06	7.130E−07
	Order	–	–	2.000	2.000
		$\tau_0 = 1/178$	$\tau_0/2$	$\tau_0/3$	$\tau_0/4$
ESVM4	$e_2^{\tau,h}(T=1)$	3.646E−10	2.281E−11	4.543E−12	1.479E−12
	Order	–	3.999	3.979	3.901
SVM4	$e_2^{\tau,h}(T=1)$	*	9.080E−10	1.760E−10	5.568E−11
	Order	–	–	4.047	4.000
Long time: final time $T = 20$					
		$\tau_0 = 1/290$	1/2000	1/4000	1/8000
ESVM2	$e_2^{\tau,h}(T=20)$	2.740E−04	5.760E−06	1.440E−06	3.600E−07
	Order	–	2.000	2.000	2.000
SVM2	$e_2^{\tau,h}(T=20)$	*	1.405E−05	3.514E−06	8.785E−07
	Order	–	–	2.000	2.000
		$\tau_0 = 1/178$	1/1000	1/1200	1/1400
ESVM4	$e_2^{\tau,h}(T=20)$	6.927E−08	6.916E−11	3.347E−11	1.823E−11
	Order	–	4.003	3.980	3.943
SVM4	$e_2^{\tau,h}(T=20)$	*	2.959E−10	1.428E−10	7.714E−11
	Order	–	–	3.997	3.993

In the following, we shall consider the SP Eq. (2.11) with

$$\Omega = 0.9,\ \alpha = 1,\ \beta = 100,\ \gamma_x = \gamma_y = 1,\ L = 12,\ N = 192, \tag{4.12}$$

and the initial condition $\psi(\mathbf{x}, 0) = \sqrt{2/(15\pi)}\exp(-|\mathbf{x}|^2/2)$. In computation practice, we choose $M = 2$ for the ESVM2/SVM2 schemes, and $M = 4$ for the ESVM4/SVM4 schemes. The Poisson potential (2.13) is computed by the kernel truncation method with optimal zero-padding factor [38].

Example 6 (Accuracy confirmation). In this example, we compare the accuracy performance of ESVM schemes with its SVM counterparts in the temporal direction. The reference solution is obtained by ESVM4 with a very small time step $\tau = 10^{-4}$.

Table 4 shows temporal errors and convergence orders, from which one can observe the following: (i) ESVM2 and SVM2 are all second-order in time, while ESVM4 and SVM4 are fourth-order. (ii) ESVM schemes are more robust than SVM schemes. That is, SVM4 and SVM2 diverge at a larger time step $\tau_0 = 1/178$ and $\tau_0 = 1/290$ for $T = 1$ and $T = 20$, respectively, while ESVM scheme is convergent.

To compare the numerical stability, we present the maximum time step, larger than which the numerical simulation will diverge or even blow up, versus different final time T for ESVM, SVM schemes in Fig. 10. We can clearly observe that the maximum time step size of the ESVM schemes is much larger than that of the same order SVM schemes. To be more specific, the maximum time steps for ESVM4, SVM4, ESVM2 and SVM2 are $\frac{1}{160}$, $\frac{1}{275}$, $\frac{1}{274}$ and $\frac{1}{296}$ as $T = 1$.

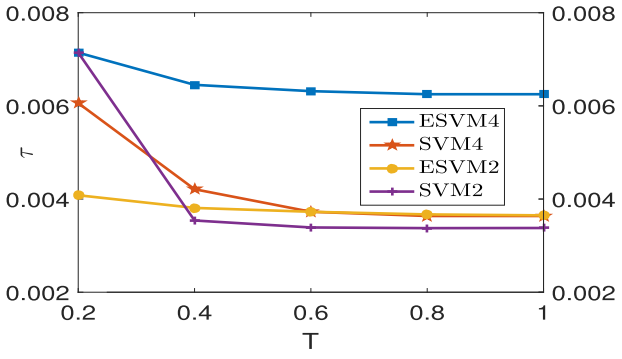

Fig. 10. Maximum time steps versus time T in Example 6.

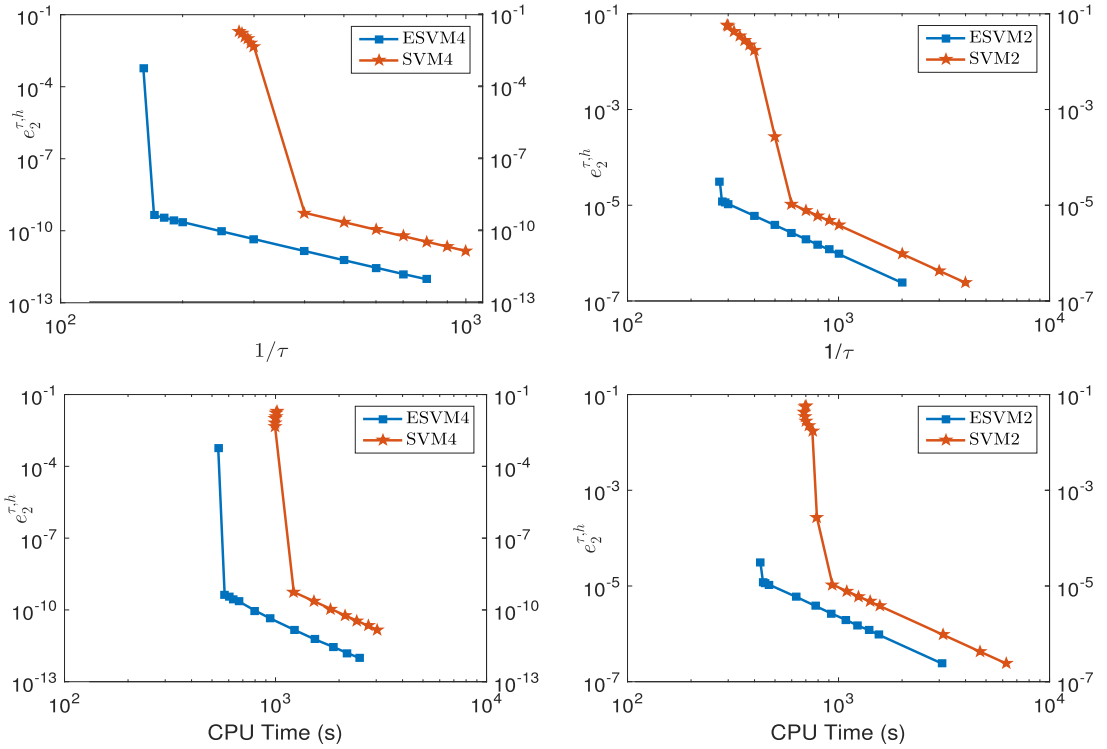

Fig. 11. Accuracies versus time steps (top row) and CPU time (bottom row) at $T = 1$ in Example 6.

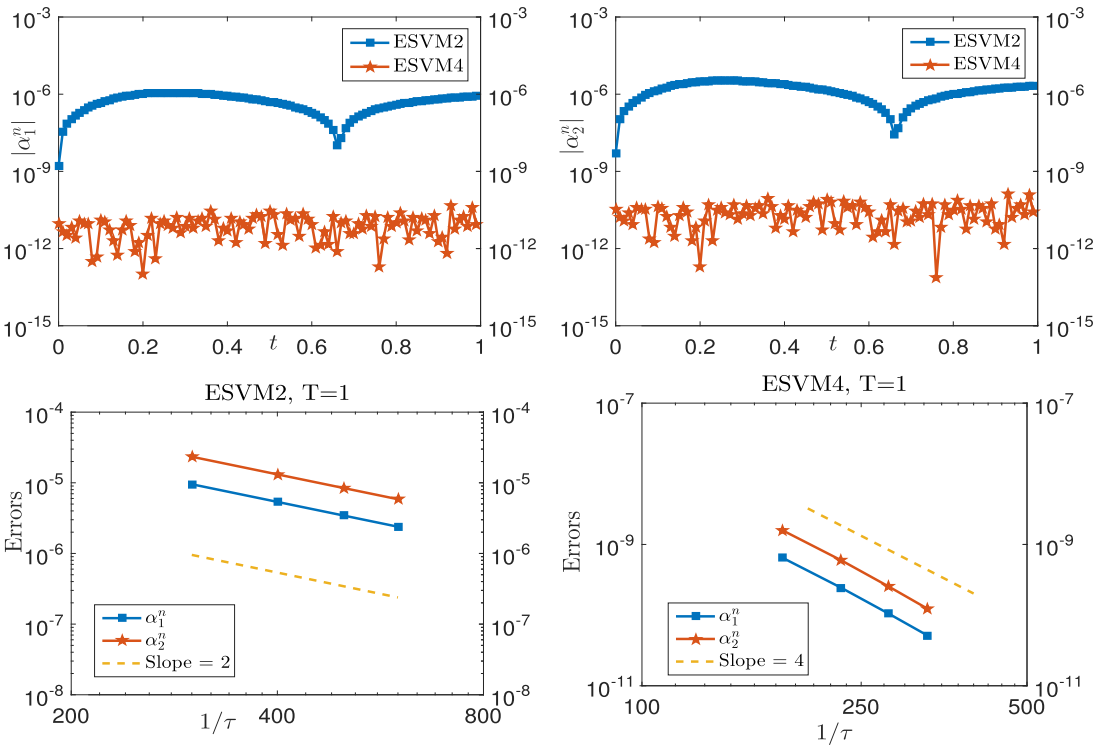

Fig. 12. The evolution (top row) and convergence order (bottom row) of the supplementary variables α_1^n & α_2^n for ESVM2 & ESVM4 in Example 6.

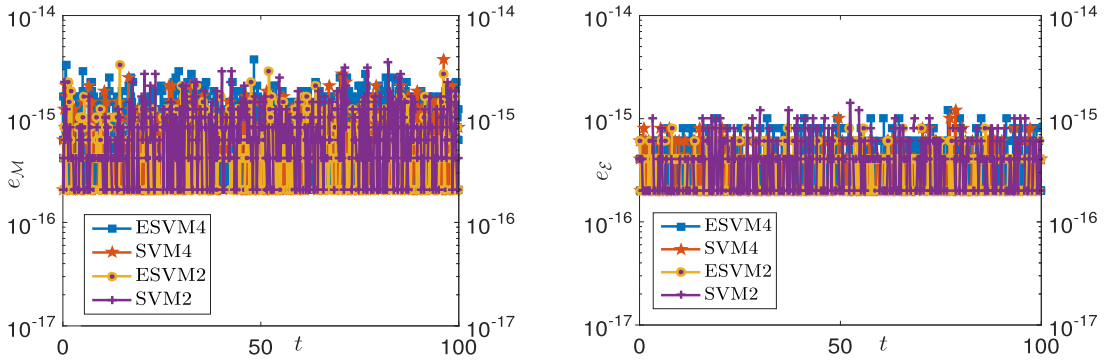

Fig. 13. Mass & energy preservation for ESVM2 & ESVM4 in Example 6.

To show efficiency superiority of ESVM, we present the accuracies versus time steps and CPU time at $T = 1$ in Fig. 11, from which one can observe that (i) For a fixed accuracy, the time step size of ESVM scheme is much larger than that of same order SVM schemes. (ii) For a given time step, ESVM scheme provides much smaller numerical error than the ones achieved by SVM scheme. Additionally, it is more efficient than the SVM ones.

Finally, we show the evolutions (top row) and convergence orders (bottom row) of the supplementary variables α_1^n and α_2^n provided by ESVM scheme in Fig. 12, and present the relative errors of mass and original energy obtained by ESVM/SVM scheme in Fig. 13. The results clearly indicate that (i) the supplementary variables remains close to zeros, and the supplementary variables in ESVM2 and ESVM4 exhibit second-order accuracy and fourth-order accuracy in time, respectively. (ii) ESVM/SVM scheme conserves the mass and original energy very well with numerical errors approaching machine-precision.

5. Conclusions

In this paper, we have proposed ESVM approach for complex-valued Hamiltonian PDEs, which provides a robust mathematical framework for developing efficient high-order exponential energy-preserving algorithms. The core idea involves rewriting the original model, coupled with conservation laws, into a structurally stable, extended system based on the Lawson transformation. Subsequently, utilizing high-order prediction-correction methods in time and spectral methods in space, we construct a class of fully discrete exponential schemes that preserve multiple conserved quantities. Ample numerical results are presented to confirm the accuracy, efficiency and long-time evolution of mass and energy conservation laws for the GP equation, along with applications to rotating multi-component BECs and Schrödinger-Poisson equation. The proposed method can be easily extended to compute dynamics of relevant BECs, such as the rotating dipolar and spinor BECs.

CRediT authorship contribution statement

Yuezheng Gong: Supervision, Methodology, Formal analysis; **Chaolong Jiang:** Writing – original draft, Methodology, Data curation; **Yong Zhang:** Writing – review & editing, Supervision, Data curation.

Data availability

Data will be made available on request.

Declaration of competing interest

The authors declare that they have no known competing financial interests or personal relationships that could have appeared to influence the work reported in this paper.

Acknowledgments

The authors would like to express sincere gratitude to the two referees for their insightful comments and suggestions. This work is partially supported by the National Key R&D Program of China No. 2024YFA1012803 (Y. Zhang), the National Natural Science Foundation of China Grant nos. 12271252 (Y. Gong), 12261097 (C. Jiang) and 12271400 (Y. Zhang), the Natural Science Foundation of Jiangsu Province Grant no. BK20220131 (Y. Gong), the Yunnan Fundamental Research Projects Grant no. 202501AT070446 (C. Jiang), and the Basic Research Fund of Tianjin University Grant no. 2025XJ21-0010 (Y. Zhang).

References

[1] Y. Gong, Q. Hong, Q. Wang, Supplementary variable method for thermodynamically consistent partial differential equations, Comput. Methods Appl. Mech. Eng. 381 (2021) 113746.
[2] Q. Hong, Q. Wang, Y. Gong, High-order supplementary variable methods for thermodynamically consistent partial differential equations, Comput. Methods Appl. Mech. Eng. 416 (2023) 116306.
[3] M. Hochbruck, A. Ostermann, Exponential integrators, Acta Numer. 19 (2010) 209–286.
[4] T.J. Bridges, S. Reich, Numerical methods for Hamiltonian PDEs, J. Phys. A 39 (2006) 5287–5320.
[5] M. Dahlby, B. Owren, A general framework for deriving integral preserving numerical methods for PDEs, SIAM J. Sci. Comput. 33 (2011) 2318–2340.
[6] E. Hairer, C. Lubich, G. Wanner, Geometric Numerical Integration: Structure-Preserving Algorithms for Ordinary Differential Equations, Springer-Verlag, Berlin, second ed., 2006.
[7] R.I. Mclachlan, G.R.W. Quispel, N. Robidoux, Geometric integration using discrete gradients, Philos. Trans. R. Soc. Lond. A 357 (1999) 1021–1045.
[8] G.R.W. Quispel, D.I. Mclaren, A new class of energy-preserving numerical integration methods, J. Phys. A 41 (2008) 45206.
[9] E. Hairer, Energy-preserving variant of collocation methods, J. Numer. Anal. Ind. Appl. Math. 5 (2010) 73–84.
[10] L. Brugnano, F. Iavernaro, D. Trigiante, Hamiltonian boundary value methods (energy preserving discrete line integral methods), J. Numer. Anal. Ind. Appl. Math. 5 (2010) 17–37.
[11] D. Furihata, Finite difference schemes for $\frac{\partial u}{\partial t} = (\frac{\partial}{\partial x})^{\alpha} \frac{\delta G}{\delta u}$ that inherit energy conservation or dissipation property, J. Comput. Phys. 156 (1999) 181–205.
[12] E. Celledoni, V. Grimm, R.I. Mclachlan, D.I. Mclaren, D. O'neale, B. Owren, G.R.W. Quispel, Preserving energy resp. dissipation in numerical PDEs using the "average vector field" method, J. Comput. Phys. 231 (2012) 6770–6789.
[13] L. Brugnano, Y. Sun, Multiple invariants conserving Runge–Kutta type methods for Hamiltonian problems, Numer. Algor. 65 (2014) 611–632.
[14] M. Dahlby, B. Owren, T. Yaguchi, Preserving multiple first integrals by discrete gradients, J. Phys. A 44 (2011) 305205.
[15] J.D. Lawson, Generalized Runge–Kutta processes for stable systems with large Lipschitz constants, SIAM J. Numer. Anal. 4 (1967) 372–380.
[16] Y. Li, X. Wu, Exponential integrators preserving first integrals or Lyapunov functions for conservative or dissipative systems, SIAM J. Sci. Comput. 38 (2016) 1876–A1895.
[17] X. Shen, M. Leok, Geometric exponential integrators, J. Comput. Phys. 382 (2019) 27–42.
[18] E. Celledoni, D. Cohen, B. Owren, Symmetric exponential integrators with an application to the cubic Schrödinger equation, Found. Comput. Math. 8 (2008) 303–317.
[19] A. Bhatt, B.E. Moore, Structure-preserving exponential Runge–Kutta methods, SIAM J. Sci. Comput. 39 (2017) 593–A612.
[20] L. Mei, L. Huang, X. Wu, Energy-preserving exponential integrators of arbitrarily high order for conservative or dissipative systems with highly oscillatory solutions, J. Comput. Phys. 442 (2021) 110429.
[21] L. Li, A new symmetric linearly implicit exponential integrator preserving polynomial invariants or Lyapunov functions for conservative or dissipative systems, J. Comput. Phys. 449 (2022) 110800.
[22] J. Shen, J. Xu, J. Yang, The scalar auxiliary variable (SAV) approach for gradient flows, J. Comput. Phys. 353 (2018) 407–416.
[23] X. Yang, J. Zhao, Q. Wang, Numerical approximations for the molecular beam epitaxial growth model based on the invariant energy quadratization method, J. Comput. Phys. 333 (2017) 104–127.
[24] C. Jiang, J. Cui, X. Qian, S. Song, High-order linearly implicit structure-preserving exponential integrators for the nonlinear Schrödinger equation, J. Sci. Comput. 90 (2022) 66.
[25] D. Li, X. Li, Relaxation exponential Rosenbrock-type methods for oscillatory Hamiltonian systems, SIAM J. Sci. Comput. 45 (2023) 2886–A2911.
[26] Q. Cheng, C. Liu, J. Shen, A new Lagrange multiplier approach for gradient flows, Comput. Methods Appl. Mech. Eng. 367 (2020) 113070.
[27] Q. Cheng, J. Shen, Global constraints preserving scalar auxiliary variable schemes for gradient flows, SIAM J. Sci. Comput. 42 (2020) 2489–A2513.
[28] W. Bao, Y. Cai, Optimal error estimates of finite difference methods for the Gross–Pitaevskii equation with angular momentum rotation, Math. Comput. 82 (2013) 99–128.
[29] X. Antoine, J. Shen, Q. Tang, Scalar auxiliary variable/Lagrange multiplier based pseudospectral schemes for the dynamics of nonlinear Schrödinger/Gross–Pitaevskii equations, J. Comput. Phys. 437 (2021) 110328.
[30] C. Besse, G. Dujardin, I. Lacroix–Violet, High order exponential integrators for nonlinear Schrödinger equations with application to rotating Bose–Einstein condensates, SIAM J. Numer. Anal. 55 (2017) 1387–1411.
[31] W. Bao, S. Jiang, Q. Tang, Y. Zhang, Computing the ground state and dynamics of the nonlinear Schrödinger equation with nonlocal interactions via the nonuniform FFT, J. Comput. Phys. 296 (2015) 72–89.
[32] X. Liu, X. Meng, Q. Tang, Y. Zhang, High-order compact splitting spectral methods for the rotating spin-1 Bose–Einstein condensates in a magnetic field, Math. Models Methods Appl. Sci. 35 (9) (2025) 2013–2045.
[33] M. Calvo, D. Hernández-Abreu, J.I. Montijano, L. Rández, On the preservation of invariants by explicit Runge–Kutta methods, SIAM J. Sci. Comput. 28 (2006) 868–885.
[34] Q. Cheng, J. Shen, C. Wang, Unique solvability and error analysis of a scheme using the Lagrange multiplier approach for gradient flows, SIAM J. Numer. Anal. 63 (2025) 772–799.
[35] J. Shen, T. Tang, Spectral and High-Order Methods with Applications, Beijing, Science Press, 2006.
[36] X. Antoine, A. Levitt, Q. Tang, Efficient spectral computation of the stationary states of rotating Bose–Einstein condensates by preconditioned nonlinear conjugate gradient methods, J. Comput. Phys. 343 (2017) 92–109.
[37] X. Antoine, Q. Tang, Y. Zhang, A preconditioned conjugated gradient method for computing ground states of rotating dipolar Bose–Einstein condensates via kernel truncation method for dipole-dipole interaction evaluation, Commun. Comput. Phys. 24 (2018) 966–988.
[38] X. Liu, Q. Tang, S. Zhang, Y. Zhang, On optimal zero-padding of kernel truncation method, SIAM J. Sci. Comput. 46 (2024) A23–A49.
[39] Y. Gong, J. Cai, Y. Wang, Multi-symplectic Fourier pseudospectral method for the Kawahara equation, Commun. Comput. Phys. 16 (2014) 35–55.